University of São Paulo
FFCLRP - Department of Physics
Postgraduate in Physics applied to Medicine and Biology

Detecção de alterações relacionadas ao câncer de mama através de sensores de carga ou de massa acoplados a monocamadas de DNA

(Detection of changes related with breast cancer using charge sensors or mass sensors coupled to DNA monolayers)

MARINA RIBEIRO BATISTUTI

Thesis submitted to Faculty of Philosophy, Sciences and Literature of University of São Paulo, as part of the requirements for the degree of Doctor in Science. Area: Physics applied to Medicine and Biology.

Ribeirão Preto - SP
2017

MARINA RIBEIRO BATISTUTI

Detecção de alterações relacionadas ao câncer de mama através de sensores de carga ou de massa acoplados a monocamadas de DNA

Thesis submitted to Faculty of Philosophy, Sciences and Literature of University of São Paulo, as part of the requirements for the degree of Doctor in Science.

Concentration area:
Physics applied to Medicine and Biology.

Supervisor:
Marcelo Mulato.

Co-supervisor:
Paulo Roberto Bueno.

Versão corrigida
Versão original disponível na FFCLRP-

Ribeirão Preto - SP
2017

FICHA CATALOGRÁFICA

Batistuti, Marina Ribeiro

Detecção de alterações relacionadas ao câncer de mama através de sensores de carga ou de massa acoplados a monocamadas de DNA / Marina Ribeiro Batistuti; supervisor Marcelo Mulato. Ribeirão Preto - SP, 2017.

122 f.:il.

Thesis (Ph.D. - Program of Postgraduate in Physics applied to Medicine and Biology) - Faculty of Philosophy, Sciences and Literature da University of São Paulo, 2017.

1. Electrochemical. 2. QCM. 3. DNA. 4. Aptamer.

Name: Batistuti, Marina Ribeiro

Title: Detecção de alterações relacionadas ao câncer de mama através de sensores de carga ou de massa acoplados a monocamadas de DNA

Thesis submitted to Faculty of Philosophy, Sciences and Literature of University of São Paulo, as part of the requirements for the degree of Doctor in Science.

Approved in:____/____/____.

Examiners

Prof. Dr. : ________________________ Institution: ____________
Judgment: ________________________ Signature: ____________

Prof. Dr. : ________________________ Institution: ____________
Judgment: ________________________ Signature: ____________

Prof. Dr. : ________________________ Institution: ____________
Judgment: ________________________ Signature: ____________

Prof. Dr. : ________________________ Institution: ____________
Judgment: ________________________ Signature: ____________

Prof. Dr. : ________________________ Institution: ____________
Judgment: ________________________ Signature: ____________

Dedicated in loving memory of my friend

Natalia Biziak

who supported me and this project since the beginning.

Your absence will always be felt.

Dedicado com carinho a memória da minha amiga

Natalia Biziak

que me apoiou e apoiou este projeto desde o início.

Sua ausência será sempre sentida.

Acknowledgment

This project received the necessary help and support from different areas which I will be eternally grateful.

I am deeply grateful to my supervisor Professor Marcelo Mulato, who supported this work, trusted me to develop it and encouraged me to go further. I also express my gratitude to my co-supervisor Professor Paulo Roberto Bueno, for his support and advice.

I express my warmest gratitude to Professor Pedro Estrela from University of Bath for receiving me on his lab. His guidance, insightful comments and suggestions were indispensable for this thesis. I am deeply grateful to Professor Michael Ladomery for introduced me on molecular biology and always show his passion on this subject.

All my friends and colleagues from the laboratory in Ribeirão Preto, especially Jessica Colnaghi Fernandes, Haroldo Lima Pimentel Cravo, Guilherme de Oliveria Silva, Raphael Aparecido Nascimento, Hugo José Dias Mello, Ricardo França Rocha and Fernando Mano for their help and friendship. I would like to express my gratitude to Bassam Junior, Stephanie Lisboa, Joyce Moraes and Daísy Camargo Ferreira. Thank you for allowing me to share with you the little that I know.

My friends and colleagues in the laboratory in Araraquara, especially Adriano Santos, Tiago Azevedo and Flávio Bedatty Fernandes. Thank you for all patience and help. From University of the West of England, I would like to express my gratitude to Samantha Jumbe, Elizabeth Bowler and Chigeru Wodi for all the patience and time spent with me.

From University of Bath, my intellectual debt is to Pawan Jolly, who guided me over the months there, trusted me and shared all his knowledge. I would like

to offer my special thanks to Pavel Zhurauski, Serife Ustuner, Nikhil Bhalla, Nello Formisano, Anna Miodek, Jules Hammond, Jahnavi Jha and Sunil Arya. They made the everyday life of PhD in Bath such enjoyable experience.

I would also like to express my gratitude to FAPESP for all financial support in Brazil (2013/26133-7) and in UK (2015/14403-5 and 2015/14404-1).

I owe my deepest gratitude to my parents Paschoal and Cristina, my brothers Guilherme e Nícolas and my fiancé David, who continuous supported me and encouraged over this years and made it posssible. Words will never be enough to say thank you!

Finally, to my countless friends that made my life so much happier and will be impossible to name them here!

To God, all praise, honor and glories.

Abstract

BATISTUTI, M. R. **Detection of changes related to breast cancer using charge sensors or mass sensors coupled to DNA monolayers**. 2017. 122 f. Thesis (Ph.D. - Postgraduate program in Physics applied to Medicine and Biology) - Faculty of Philosophy, Sciences and Literature, University of São Paulo, Ribeirão Preto - SP, 2017.

The electrochemical biosensor has been extensively used due to its capacity for rapid and accurate detection of a wide variety of target molecules or biomarkers. DNA hybridization sensors are based on the increase of negative charge on the electrode surface after the DNA target hybridize to the immobilized probes. The development of this platform requires first an understanding of the immobilization process and optimization of surface probe density. In this thesis the electron transfer is investigated on a label-free DNA hybridization detection by its intrinsic charge. The investigation using different immobilization buffers shows a strong dependence on their composition and concentration, and also the influence of the probe and spacer co-immobilized to obtain an organized and compact self-assembled monolayer. The probe density is determined using the chronocoulometry method with hexaammineruthenium (III) chloride, where the value is calculated from the number of cationic redox molecules electrostatically associated with the anionic DNA backbone and presented a linear relationship between thiol molar fraction and probe density from 2 to 5 x 10^{12} molecules/cm^2. The effect of hybridization was determined using electrochemical impedance spectroscopy using negatively charged ferri/ferrocyanide redox couple in solution. After probe surface density optimization, the maximum shift of charge transfer resistence (20%) upon 1 μM complementary sequence was obtained with around 25% probe fraction immobilized

on surface. This electrochemical platform developed was able to detected 100 pM of target sequence and distinguish mismatched sequences. The limit of detection is higher when compared to the literature, however, this system can be further improved by amplifing the signal. The same platform is reproduced in the quartz crystal microbalance system and with field-effect transistor, comparing the different detections. The same platform is tested using two different HER2 aptamer sequences. Biological aspects are explored for a better understanding of the system.
Key-words: 1. Electrochemical. 2. QCM. 3. DNA. 4. Aptamer.

List of Figures

List of Tables

Abbreviations

AC	Alternate current.
BioFET	Biological recognition element immobilized on FET surface.
BVD	Butterworth van Dyke.
CC	Chronocoulometry.
CV	Cyclic voltammetry.
DNA	Deoxyribonucleic acid.
dsDNA	Double strand DNA.
DTT	Dithiothreitol.
EDTA	Ethylenediaminetetraacetic acid.
EIS	Electrochemical impedance spectroscopy.
EGFET	Extended Gate Field-Effect Transistor.
FET	Field-effect transistor.
IHP	Inner Helmholtz phase.
ISFET	Ion Sensitive Field-Effect Transistor.
LNA	Locked nucleic acid.
LOD	Limit of detection.
MCH	6-mercapto-1-hexanol.

miRNA	MicroRNA.
MOSFET	Metal-oxide-semiconductor field-effect transistor.
OHP	Outer Helmholtz phase.
PB	Potassium phophate buffer.
PBS	Phosphate-buffered saline.
PCR	Polymerase chain reaction.
PNA	Peptide nucleic acid.
QCM	Quartz cristal microbalance.
RC	Resistor Capacitor.
RNA	Ribonucleic acid.
SAM	Self-assembled monolayer.
ssDNA	Single strand DNA.
tDNA	target DNA.
TE	Tris with EDTA.
WB	Western Blot.

Nomenclature

A	Area.
C	Complex capacitance.
C'	Real capacitance.
C"	Imaginary capacitance.
C_0	Concentration of species oxidized.
C_1	Capacitor related to the stored energy in the oscillation.
C_D	Diffuse-layer capacitance.
C_{dl}	Double layer capacitance.
C_H	Helmholts-layer capacitance.
C_Q	Constant of the quartz.
d	Thickness of dielectric layer.
D	Dissipation factor.
D_O	Diffusion coefficients of oxidised form .
D_R	Diffusion coefficients of reducer form.
E	Potential.
E_0	Standard electrode potential or potential peak amplitude.
E_{ap}	Anode peak potential.

E_{cp}	Cathode peak potential.
E_f	Reverse potential.
E_i	Initial potential.
F	Faraday constant.
f	Frequency.
f_q	Quartz resonator frequency.
I or i	Current.
I_0	Peak current amplitude.
I_{ap}	Anode peak current.
I_{cp}	Cathode peak current.
L_1	Inductor related to the inertial component of the oscillation.
n	Number of electrons or overtone.
Q	Total charge.
Q_{ads}	Adsorbed charge.
Q_c	Double layer charge.
Q_{diff}	Cumulative charge.
R	Gas constant or Resistance.
R_1	Dissipation of the oscillation energy.
R_{ct}	Charge transfer resistance.
R_{dl}	Double layer resistance.
R_S	Solution resistance.
T	Temperature.

t	Time.
Y	Admitance.
Z	Complex impedance.
Z' or Z_{Re}	Real impedance.
Z"or Z_{Im}	Imaginary impedance.
Z_C	Impedance of a capacitor.
Z_R	Impedance of a resistor.
Z_{RC}	Impedance of RC system.
Z_W	Warburg impedance.
Γ_{DNA}	Probe surface density.
Γ_R	Amount of redox marker confined near the electrode surface.
Δ_D	Dissipation factor shift.
ΔE_p	Distance separation of peak potential.
Δ_f	Frequency shift.
Δ_m	Change of mass.
ε_0	Permittivity of free space.
ε_m	Dieletric constant of SAM.
η_l	Liquid density.
θ	Phase angle from potential.
μ_q	Shear modulus.
ρ_l	Liquid viscosity.
ρ_q	Quartz density.

ϕ	Phase angle from current.
ω	Angular frequency.

Contents

Chapter 1

Introduction

1.1 Introduction

In April 1953 James Watson and Francis Crick proposed in a simple article the correct double helix model for DNA structure through x-ray diffraction [1]. This discovery has paved the way for all understanding of how genetic information is stored and transmitted. Almost 10 years later, Eley and Spivey suggested that DNA could conduct charge based on its similarity to one-dimensional structures of aromatic crystals [2]. Since then, the interest in the "molecule of life" has increased.

The oligonucleotides detection have been explored in many research and technological fields from forensics to medical diagnostics. There is a significant need for devices with high sensitive and selective detection, and also low cost, giving a direct eletronic signal and that can easily be miniaturized to portable devices for point-of-care [3]. For this, biosensors have been investigated once they can provide specific quantitative information using a biological recognition element directly in contact with a transduction element. Specifically, a DNA biosensor presents a single strand nucleic acid working as biological recognition element [4]. Different detection strategies have been applied, however there are just a few commercial devices. Problems with reproducibility and sensitivity are the major concern due to surface attachment and hybridization.

The electrochemical tranducer attracted a lot of attention since it gives an eletronic signal directly, with low cost and can easily be miniaturized, enabling the development of portable devices [5]. Also, several approaches to signal transduction presented promising results [6]. The development of this biosensors with broad

potential for exploitation and, therefore, eliminate problems of reproducibility and sensitivity.

Therefore, electrochemical biosensors are one of the most promising platforms with the potential to achieve these goals and have already been used to detect different analytes, including, e.g., disease biomarkers [7] and proteins [8], microRNAs [6], microorganisms in water [9], toxins in food samples [10] and biomolecules in human serum [11].

1.2 Aim of the study

The aim of the thesis is to develop a DNA/DNA biosensor that can be easily expanded to microRNA, PNA or aptamer systems. The characterization and detection are based mainly on DNA charge using electrochemical techniques, but also will be compared with piezoeletric and field-effect techniques. The development involves a deep understanding of DNA immobilization, electrochemical double-layer components and how the biorecognition event affects the double-layer.

The electrochemical biosensor platform focuses on synthetic DNA oligonucleotides immobilized via thiol groups onto gold electrodes surface, where the single strand DNA has intrinsic negative charge due to its phosphate groups. Hybridization of the complementary sequence increase the negative charge in the electrode surface and the detection of this label-free system through electrochemical impedance spectroscopy requires a redox marker in solution. However, the same system can be further amplified with gold nanoparticles or redox intercalators and modulated by other electrochemical techniques, as square wave voltammetry or electrochemical capacitance spectroscopy.

The biosensor platform was tested with piezoeletric and field-effect transduction. In the first case, the immobilization strategy was reproduced on the top of a quartz cristal covered with gold. The hybridization increases the mass, decreasing the resonance frequence. On the other hand, field-effect tranducers are able to detect directly the charge variation. For this, gold electrodes were connected to the gate of the FET. The limits of detection for all techniques are compared.

To show that the DNA/DNA biosensor can be expanded to other systems

with a similar immobilization strategy, an aptasensor is developed using different DNA sequences to detect a target protein. Surface plasmon resonance confirms the protein binding. All the electrochemical biosensors were modeled by an equivalent eletric circuit.

1.3 Overview of the thesis

Chapter 2 introduces the basic theories and relevant aspects for the DNA biosensors employed in the study. It starts with an overview of the system, reviewing the electrochemical double layer, the electrochemical cell and the main techniques involved. It is followed by the theories that describe piezoeletric and field-effect transducers.

The study of probe immobilization is presented in chapter 3, which includes: gold electrodes cleaning, determination of surface roughness, sample preparation and the self assembled monolayers (SAM). All these steps proved to be necessary in order to develop a compact and stable monolayer and reproducible results. Immobilization procedure was optimized and will be discussed in detail.

In chapter 4 electrochemical impedance spectroscopy (EIS) of modified electrode surfaces is studied based on the charge effect. To achieve better sensitivity and lower detection limit, the SAM was optimized using electrochemical methods and modeled according to an eletric circuit to understand the significance of all elements in the mixed structure and solutions. Also included a brief introduction on the microRNA sequence used and its role as a biomarker. A brief comparative study of DNA hybridization sensors using quartz crytal microbalance and field effect transistor signal is presented.

Chapter 5 introduces the aptasensors using different DNA sequences for HER2 protein and its importance as a biomarker. The same immobilization strategy on the top of gold electrodes was investigated using EIS. The density of aptamers on the surface was optimized to achieve limits of detection close to the clinically relevante values.

The final conclusions are presented in chapter 6 with suggestions on how this work can be improved and extended to other biosensors systems.

At the same time, it is important to understand biological aspects of targets molecules. The appendix in the end of the thesis presents a cancer cell line culture and how to extract specific microRNAs. Different biological techniques can be used to describe and evaluate this material. For microRNA quantification, polymerase chain reaction (PCR) amplification is the main technique. Some important aspects will be discussed to correlate human levels with the biosensors limits of detection.

Chapter 2

Theories and Principles

This chapter briefly describes the relevant theories and principles applied in label-free biosensors. And also, the characterization techniques employed in the study.

2.1 Electrochemical overview of the system

A DNA biosensor has a typical configuration where single-stranded probes (ssDNA) are immobilized on the electrodes. The uniform structure of DNA makes its assembly well defined. To prevent non-specific binding, small molecules called spacers, are co-immobilized with ssDNA. Gold electrodes can be easily modified with thiolated probes forming an oriented self-assembled monolayer (SAM). In this interface the critical dynamics of target capture take place. Therefore, maintaining the inherent affinity for target DNA is the key to device performance [3].

When this whole system is immersed in an electrolyte solution, a specific region is formed, the double layer. The structure of this interfacial region can affect the rates of electrode processes or, in other words, the electrical properties of this layer can affect the electrochemical measurements of the system [12].

The electrochemical system is composed of a working electrode modified with the SAM, a reference electrode and a counter electrode. The potencial is set between the reference electrode and the working electrode while the redox current between the working and counter electrodes. Figure 2.1 illustrates the electrochemical biosensor system (a) with the three electrodes correlated with the equivalent circuit (b).

In the electric circuit used to model the system, the double-layer can

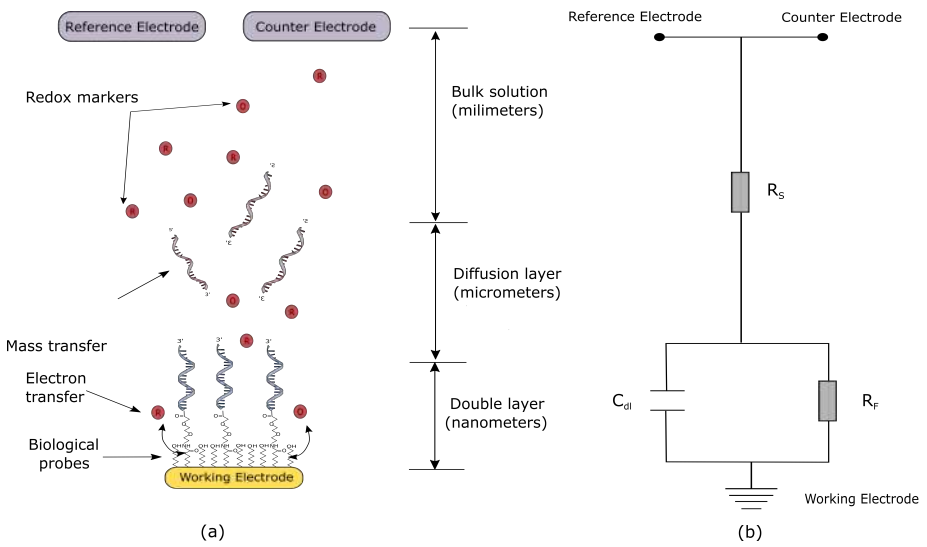

Figure 2.1: *Electrochemical DNA biosensor system. In (a) an illustration with the all the elements and processes. In (b) the equivalent electric circuit of the system.*

be compared with a capacitor (C_{dl}) in parallel with a resistance (R_{dl}). This circuit carries information concerning the double layer structure and can be electrochemically investigated. A label-free system uses a redox molecule in solution to exchange electrons with the working electrode. This process can be divided in electron transfer and mass transfer. The principles of these two processes and characterization methods are introduced to understand the DNA biosensor system.

2.2 Principles of Electrochemistry

2.2.1 Electrical Double Layer

The concept of electrical double layer was first introduced by Helmholtz in 1879. He suggested that a charged surface in contact with an electrolyte solution repels ions of the same charge and attracts their counter-ions [13]. This monolayer of electronic charge at the electrode surface and the layer of counter-ions in the electrolyte forms what has been called as electrical double layer. This structure is illustrated in Figure 2.2a and is analogous to dieletric capacitors with two plannar electrodes separated by a small distance that correspond to approximately the radius of an ion.

In 1910, Gouy and Chapman considered the double layer not as compact

as in Helmholtz rigid layer, but modified adding a diffuse double layer in which the accumulated ions, due to the Boltzmann distribution, decreases exponentially as a function of the distance from the electrode surface [14]. This model describes ions as mobile in the solution under effects of diffusion from concentration gradients and electromigration from electric potential gradient, or electric field. The result is illustrated in Figure 2.2b.

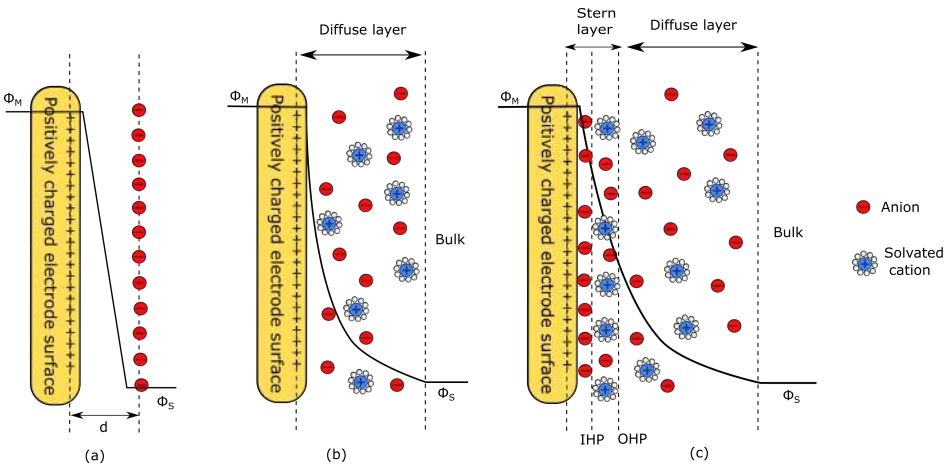

Figure 2.2: *Illustration of double layer region of an electrochemical interface according to Helmholtz in (a), Gouy-Chapmann in (b) and the Gouy-Chapman-Stern model in (c).*

However, Gouy-Chapmann treated ions as point-charges resulting in unrealistically large ion concentration at the electrode surface and consequently, overestimating the electrical double layer capacitance. A few years later, in 1924, Stern suggested that the interface electrode/solution includes both: the rigid Helmholtz layer and the diffuse layer from Gouy and Chapman, considering the finite size of ions [13]. The inner region called the Stern layer and the outer region called the diffuse layer are shown in Figure 2.2c.

2.2.2 Electrochemical Cells

The electrochemical experiments are carried out in a three-electrode cell. This arrangement is compoused of working electrode (W) where the reaction of interest occurs, the reference electrode (R) which has a known potential and large non-polarizability and the counter electrode (C), or auxiliary. All of them are immersed in an electrolyte solution, as illustrated in Figure 2.3(a). The potentiostat

applies the voltage on the reference electrode against the working electrode with a high input impedance, and consequently, the potencial will be constant and equal to the open-circuit value. At the same time, it measures the current that flows between the working electrode and the counter electrode.

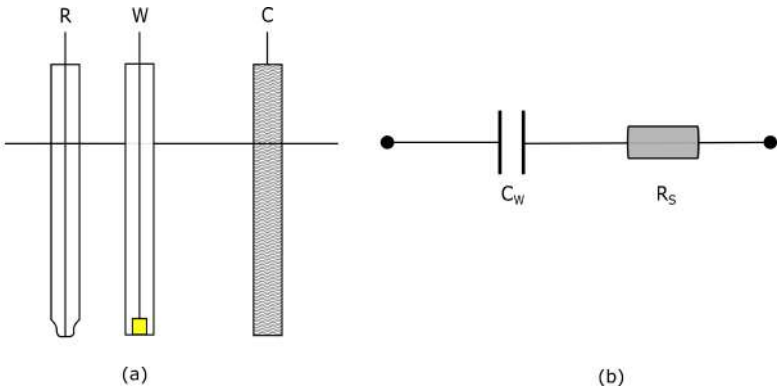

Figure 2.3: *Illustration of the electrochemical cell. In (a) the correct position between the reference, working and counter electrodes. In (b) the equivalent circuit to describe the cell with the capacitance at the working electrode (C_w) and the solution resistance (R_s).*

The electrochemical cell can also be described by an RC equivalent circuit, as shown in Figure 2.3(b). The double-layer capacitance at the working electrode is represented by C_w and the solution resistance by R_s. The separation between the electrodes affects the potencial drop. The configuration shown in Figure 2.3(a) minimises this effect [14].

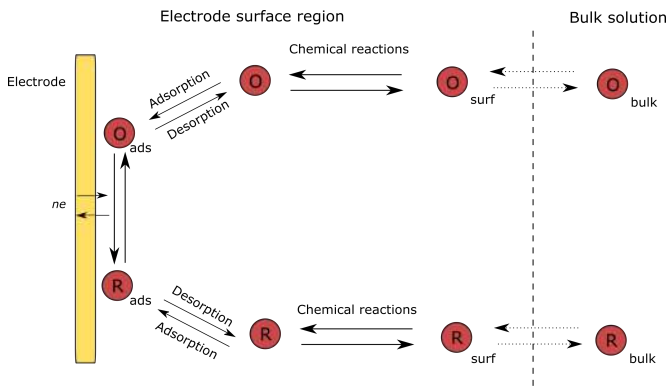

Figure 2.4: *Illustration of the mass transport from the bulk to the electrode surface, electron transfer at the electrode surface and other chemical reactions following the electron transfer.*

The reaction on the working electrode surface is composed of a series of steps that causes the conversion of the oxidized and reduced species in solution, illustrated

in Figure 2.4. The current is governed by the mass transfer rates from the bulk to the electrode surface, electron transfer at the electrode surface and other chemical reactions following the electron transfer.

2.2.3 Electrochemical characterization techniques

The electrochemical theory for each technique employed in the thesis is discribed in this section, however the details and applications are presented in the next chapters where they are applied.

Electrochemical techniques can be divided in two classes of measurement, potentiometry where the potential between two electrodes is measured, or amperometry in which the current that flows between two electrodes is measured. This thesis will focus on different methods for analysis.

2.2.3.1 Cyclic Voltammetry

Cyclic voltammetry is one of the most complex electrochemical techniques and very frequently used since it is rapid and powerful method for characterizing the electrochemical behavior of analytes that can be electrochemically oxidized or reduced [14]. It is a scanning technique in which sweeps the potential linearly between the initial potential E_i and the reverse potential E_f. [12].

Suppose that the scan starts at a negative potential, where only nonfaradaic currents, from charge or discharge of doucle layer capacitance, will flow for a while. When the potential increase and reaches close to the oxidation value (E_{pa}), the faradaic current starts to flow. As the potential continues to grow more positive, the surface concentration of species drops. When the potential moves past E_{pa} the mass transfer of analyte to the surface reaches a maximum rate, and then it declines. This can be observed in Figure 3.2(a) as the input voltage signal as the linear increase and in (b) as the positives values of current and a peaked current-potential curve like that.

Now, the potential is sweeping in a negative direction, as the potential approaches and cross E_0, the surface grows more favorable toward the neutral species. After that, the species reduces close to E_{pc}. This reversal current has a similar shape to the forward peak for essentially the same reasons. From this simple

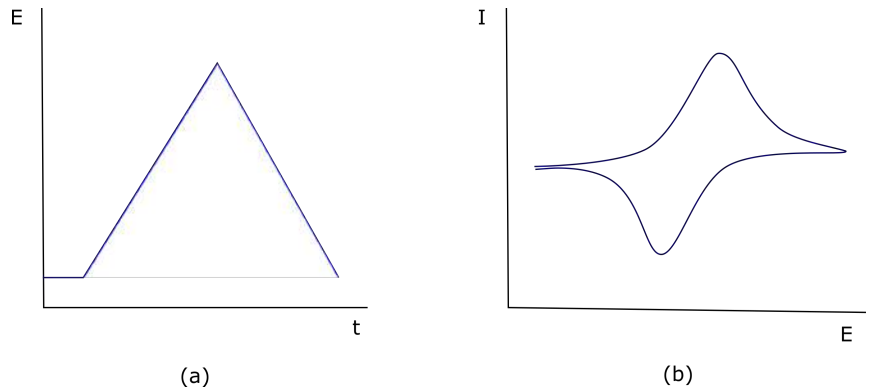

Figure 2.5: *Illustration of the cyclic voltammetry process. In (a) the potential simulation and in (b) the current response.*

graphic it is possible to extract some useful information as the E_{pc}, E_{pa} and the current of these peaks, I_{pc} and I_{pc} respectively.

In the processes of charge transfer the electrode may act as a donor (in the case of a reduction) or as a receptor (in the case of an oxidation) of electrons transferred to or from species in solution. The equilibrium state of a chemical reaction is characterized by Nernst equation (2.1):

$$E = E_0 + \frac{RT}{nF} ln \frac{D_R}{D_O} \tag{2.1}$$

which relates the potential of the electrode to the concentration of the species in solution. Nernst equation shows how the surface concentration and the electrode potential, regardless of the current flow are related. In equation 2.1, E is the applied potential difference, E_0 is the standard electrode potential, R is the gas constant, T the temperature , n the number of electrons transferred per molecule diffusing to the electrode and F the Faraday constant. D_R and D_O represent the diffusion coefficients for the reduced and the oxidized forms, respectively. At 25°C, the equation can be written as:

$$E = E_0 + \frac{0.059}{n} ln \frac{D_R}{D_O} \tag{2.2}$$

Thus, cyclic voltammetry can be applied to understand the chemical reversibility when the same reaction can take place in both directions, since the peak is a result of reaction kinetics and mass transport. Also, the shape and amplitude of the peak current can reflect the redox species reactions. In the reversible case,

the initial oxidation or reduction product is then reduced or oxidized, respectively, after inverting the potential sweep.

In order to have a reversible system, that follows Nersnt law [12], it must comply with the following conditions:

- I_p is proporcional to $v^{1/2}$
- E_p i independent of v
- E_{pa} - E_{pc} = 59/n mV
- $|_{pa}/I_{pc}| = 1$

If the reaction is reversible is possible to calculate the number of electrons transferred in the electrochemical reaction with Nersnt equation and the formal reduction potential, E_0, can also be calculated by the relation:

$$E_0 = \frac{E_{pa} + E_{pc}}{2} \tag{2.3}$$

In the case of an irreversible reaction, when the direction of the scan is inverted, the peak do not appear in the inverse scan. Also, E_p, varies linearly with log v and the irreversibility intensifies increasing scanning speed, while the values of I_{pa} and I_{pc} become different.

The intermediate region between the reversible and irreversible processes is termed quasi-reversible. In quasi-reversible systems, a reverse peak is observed, but with $\Delta E_p > 59/n$ mV.

2.2.3.2 Chronocoulometry

Chronocoulometry can be classified as a step technique, where it is possible to detect the amount of the charge passed as a function of time. It is based on Faraday's laws that are based on conservation of matter and conservation of charge. After a step the potential, the current (chronoamperometry) and the charge (chronocoulometry) through the working electrode versus time (t) is recorded.

Suppouse a reversible system with just oxidized process, the current can be described by the Cottrell equation as:

$$I(t) = \frac{nFAD_O C_O}{\pi D_O t^{1/2}} \tag{2.4}$$

where n is the number of electrons transferred, A is the electrode area, C_O is the concentration of species O. The time integral of Cottrell equation:

$$Q = \int_0^t I.dt \tag{2.5}$$

gives the cumulative charge:

$$Q_{diff}(t) = 2nFAD_O^{1/2} C_O \pi^{-1/2} t^{1/2} \tag{2.6}$$

However, it does not take into account the double layer charging and adsorption as initial conditions. The total charge should be given by:

$$Q(t) = Q_{diff}(t) + Q_c(t) + Q_{ads}(t) \tag{2.7}$$

the adsorbed amount Q_{ads} can be estimated, as:

$$Q_{ads} = nFA\Gamma_R \tag{2.8}$$

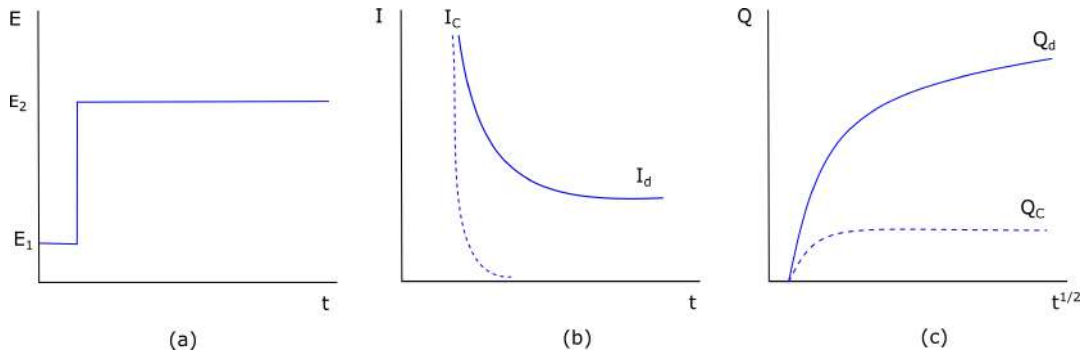

Figure 2.6: *Illustration of the cronocoulometry from the cronoamperometry. In (a) the step potential from E_1 to E_2 over the time. In (b) the current response over the time and in (c) the charge vs. time$^{1/2}$ to extract the surface density information.*

Chronocoulometric curves start when species are electrochemically inactive at a first potencial E_1 and are reduced at a second potencial E_2, illustrated in Figure

2.6(a). The experiment have to be repeated in the absence of redox species. It is important to note that in this systems just one form of the redox couple is present.

Figure 2.6(b) shows the cronoamperometry while Figure 2.6c shows the cronocoulometry. Dashed curves correspond to capacitive current and charge respectively and straight line correspond to diffusional current and charge. From Figure 2.6(c) the Q_{diff}(t) and the Q_{ads}(t) can be estimated.

2.2.4 Impedance techniques

The amperometric methods apply a large perturbation on the system being suitable for electrode kinetics investigation, however, these perturbations drive the system to a condition far from equilibrium, and what is observed as response is a transient signal [12]. Small perturbations of the electrode state are possible with an alternating signal of small amplitude. Thus, techniques based on impedance represents a powerful tool for investigation of electrical properties of materials and interfaces of conducting electrodes [14]. The theory of this section will show the analogies between the electrochemical cell and elements of an eletric circuit, as resistors and capacitors.

2.2.5 Electrochemical Impedance Spectroscopy

Impedance, in electrical terms, can be describe as the complex ratio betwen voltage and current in an alternating current (AC) circuit. Impedance extends the concept of resistance because it has magnitude and phase terms, unlike resistance, which consider only magnitude. Therefore, electrochemical impedance spectroscopy (EIS) is a technique where the electrode impedance is measured as a function of the frequency of the AC source.

Alternating current or voltage (AC) means that the current or voltage varies with time in a periodic way. Figure 2.7 shows a periodic voltage wave. The frequency (f) is the number of cycles completed in one second.

The open circuit potential (OCP), the potential at which there is no current, is applied on the system. The potential E can be described as purely sinusoidal,

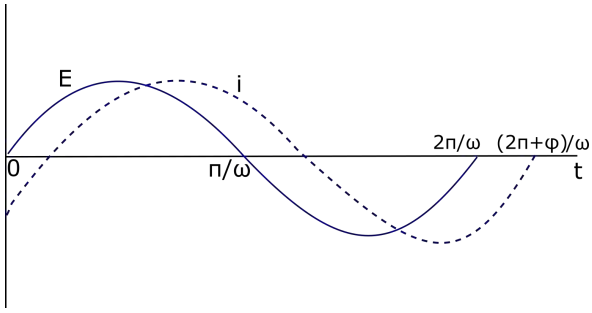

Figure 2.7: *Illustration of the potential and current waves. In black a period of the potential (E) wave and, in blue, the a period of the current wave with a shift ϕ from the E.*

being the easiest to work mathematically:

$$E(t) = E_0 sin(\omega t + \theta) \tag{2.9}$$

where E_0 represent the peak amplitude, ω the angular frequency (rad/s or 2π times the frequency in Hz) and θ phase angle (rad). Similary, the equation for a sinoidal current wave is:

$$I(t) = I_0 sin(\omega t + \phi) \tag{2.10}$$

In this case, I_0 is the amplitude of the sinusoidal current wave and ϕ is the phase angle.

Considering first the resistors in an AC circuit. The resistence through the resistor based on Ohm's law, is:

$$R = \frac{E(t)}{I(t)} \tag{2.11}$$

Since there is no angular difference, $\phi = \theta$.

Now, considering the capacitor in AC circuit. The current through a pure capacitor leads the voltage drop across this capacitor by 90°. If we consider a resistor-capacitor circuit, is possible to rewrite equations 2.9 and 2.10 as:

$$E(t) = E_0 sin(\omega t) \tag{2.12}$$

$$I(t) = I_0 sin(\omega t + 90^o) \tag{2.13}$$

The same relation can be display in complex notation:

$$\mathbf{E} = E_0 e^{i0^o} \tag{2.14}$$

$$\mathbf{I} = I_0 e^{i90^o} \tag{2.15}$$

which are defined as phasors, complex number representing a sinusoidal function. To distinguish phasor from other complex numbers, they are printed in bold. The complex number eliminated the time dependency .

Different from resistence, impedance extends the concept of resistance being a complex quantity. The complex impedance Z can be written in the rectangular form:

$$Z = Z_{re} + iZ_{im} \tag{2.16}$$

where Z_{re} (or Z') represents the real part and Z_{im} (or Z") represents the imaginary part. The impedance spectrum of an electrochemical system can be presented in Nyquist plot, which are representations of impedance as a function of frequency, where Z_{re} is represented in X axis and Z_{im} in the Y axis. More details of Nyquist diagram will be discussed in the end of this section.

Mathematicaly, the current-voltage relationship in impedance can be expressed, according to Ohm's law, as:

$$Z = \frac{E(t)}{I(t)} \tag{2.17}$$

The AC impedance of a resistor (Z_R) in the complex plane can be expressed as:

$$Z_R = \frac{E_0 sin(\omega t + \theta)}{I_0 sin(\omega t + \phi)} = R \tag{2.18}$$

The impedance of a capacitor (Z_C) in the complex plane can be expressed as:

$$Z_C = \frac{E_0 sin\omega t}{I_0 sin(\omega t + 90^o)} = \frac{E_0 e^{i0^o}}{I_0 e^{i90^o}} = \frac{E_0 e^{i0^o}}{\omega C V_0 e^{i90^o}} = \frac{e^{i(-90^o)}}{\omega C} \tag{2.19}$$

To simplify with Euler's relation:

$$e^{i(-90^o)} = cos(-90^o) + isin(-90^o) \tag{2.20}$$

$$Z_C = \frac{1}{i\omega C} \tag{2.21}$$

These circuit elements, resistence and capacitance, can be related through equivalent circuits. Considering two RC circuits; in the first, resistence and capacitance are in serie, in the second in parallel. In a series RC circuit, the overall impedance is expressed as the sum of the individual impedances:

$$Z_{RC} = R + \frac{1}{i\omega C} \tag{2.22}$$

Figure 2.8 shows a graphical representation of the impedance in the complex Nyquist plane as a straight vertical line for the RC circuit in serie, according to equation 2.22.

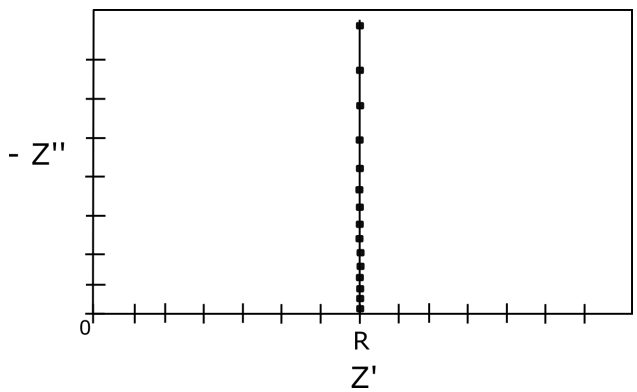

Figure 2.8: *Nyquist example of a RC circuit in serie.*

The second case, in a parallel circuit, the overall impedance can be express as:

$$\frac{1}{Z_{RC}} = \frac{1}{Z_R} + \frac{1}{Z_C} \tag{2.23}$$

$$\frac{1}{Z_{RC}} = \frac{1}{R} + \frac{i\omega C}{1} \tag{2.24}$$

Rewriting this relation above and separating the real and complex.

$$Z_{RC} = \frac{R}{1+(\omega RC)^2} - i\frac{\omega R^2 C}{1+(\omega RC)^2} \tag{2.25}$$

The first part of the equation 2.25 is real (Z_{re}) and the second is imaginary (Z_{im}). At low frequency ωRC « 1, so $Z_{re} \approx$ R and $Z_{im} \approx 0$. In this case, the RC circuit acts as a resistor. On the other hand, at high frequency ωRC »1, $Z_{re} \approx 0$ and $Z_{im} \approx \frac{1}{\omega C}$ the RC circuit acts as a capacitor.

Now, to simplify Eq. 2.25, it can be written as:

$$(Z_{re} - \frac{R}{2})^2 + Z_{im}^2 = (\frac{R}{2})^2 \tag{2.26}$$

The last equation represents a half-circle curve in the complex plane as in Figure 2.9 where the curve has radius of R/2 and circle centre of (R/2, 0).

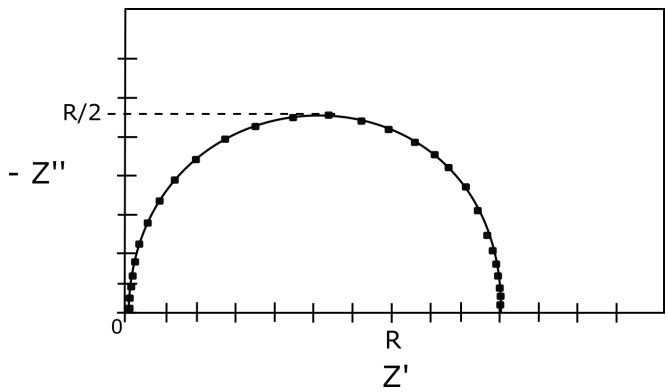

Figure 2.9: *Nyquist example of a RC circuit in parallel.*

The EIS is frequently used to evaluate the charge-transfer parameters and for studies of double-layer structure. The equivalent circuit should represent the electrochemical system as best as possible considering at least the electrolyte resistance, a double-layer capacity, and the impedance of the Faradaic or non-Faradaic process.

The most common and simple model of an electrochemical interface is the Randles circuit show in Figure 2.10a. This circuit is composed by electrolyte resistance or solution resistance (R_S), the double-layer capacitance (Cdl) and the charge transfer resistance (R_{ct}) that is the charge transfer resistance of the electrode process.

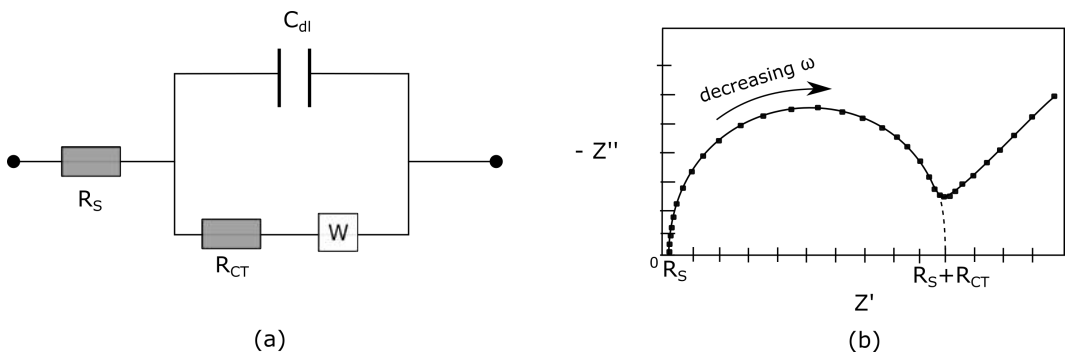

Figure 2.10: *The electrochemical interface model. In (a) the Randles circuit and the correspond Nyquist curve in (b). R_e correpond to electrolyte resistance or solution resistance, Cdl the double-layer capacitance and R_{ct} the charge transfer resistance telated to the electrode process.*

As already discussed above, the high frequency is associated with the R_S, while the low frequency corresponds to the sum of the R_{ct} and R_s and the diameter of the semicircle correspond to the R_{ct}. The Warburg impedance (Z_W) is due to the diffusion to and from the electrode in the charge transfer and, on Nyquist plot, is a line at an angle of approximately 45°. Therefore, the theory try to interpret the equivalent resistance and capacitance values in terms of interfacial phenomena.

2.2.6 Electrochemical Capacitance Spectroscopy

All the theory presented above show the electrochemical interface without any modifications on the electrode surface. The presence of films adsorbed on the surface introduces new capacitance and resistance contributions to the system that affect the electrochemical responces.

One of the most simple models for electrode modifications is the organized monolayers, or self-assembled monolayer (SAM), which are single molecules, forming nanometer thick films with common orientation, aligned on a surface. The SAM are considered as a dielectric layers on top of the electrode and are typically modeled as a parallel plate capacitor. Mathematically, a capacitor is describe as:

$$C = \frac{\varepsilon_m \varepsilon_0 A}{d} \tag{2.27}$$

where ε_m is related to the dielectric constant of the SAM, ε_0 the permittivity of free space, d is the thickness of the dielectric layer (or the SAM) and A the

electrode area. The electronic blocking of these SAMs can also be studied through equivalent circuits and EIS measures.

In a classical approach, C_{dl} is the resultant capacitance formed by the two series capacitances as:

$$\frac{1}{C_{dl}} = \frac{1}{C_H} + \frac{1}{C_D} \tag{2.28}$$

where C_H in the Helmholts-layer capacitance and C_D the diffuse-layer capacitance. For label-free SAM, the EIS measurement is normally performed in a solution with a redox marker. In these case, C_D, or faradaic capacitance, has more influence in the final result. However, for label-free SAM without redox marker in the electrolyte solution or with a redox probe confined in the SAM, the C_H component stands out, giving information of intrinsic properties of the monolayer, or the storage characteristics of the interface.

The capacitance information can be mathematically extracted from the EIS. Admittance (Y) the ability of a circuit to conduct an AC. The inverse of impedance, expressed as:

$$\mathbf{Y} = \frac{1}{\mathbf{Z}} = Y_0 e^{i\phi} = Y_{re} + iY_{im} \tag{2.29}$$

From equation 2.29, the complex capacitance can be define as:

$$\mathbf{C} = \frac{\mathbf{Y}}{i\omega} = \frac{Y_{im}}{\omega} - \frac{iY_{re}}{\omega} = C_{re} + iC_{im} \tag{2.30}$$

The result as complex capacitance can be plot similar to Nyquist.

2.3 Principles of Piezoelectricity

Piezoelectricity from the Greek (piezin) means to press and the electricity that is generated by the pressure [15]. In this way, piezoelectric effect is the ability of certain materials to generate electric charge in response to applied mechanical stress. The reversibility, where the materials has the converse piezoelectric effect (the generation of stress when an electric field is applied) is also one of the characteristics.

2.3.1 Quartz Crystal Microbalance

The piezoelectric quartz crystal microbalance (QCM) is an ultrasensitive weighting device, consisting of a disk of single quartz crystal, with metal electrodes deposited on each side of the disk [16]. When the crystal is connected to an external driving oscillator circuit it can oscillates at its resonant frequency (f). QCM works as a balance: any mass added to the electrode induces a frequency shift (Δ_f) lineraly related to the change of mass (Δ_m).

In 1959, Sauerbrey was the first to recognize the potential usefulness of QCM and demonstrate (in vacuum) [17], as:

$$\Delta_m = -\frac{C_Q}{n}\Delta_f \tag{2.31}$$

where C_Q is a constant related with the thickness and intrinsic properties of the quartz and n is the overtone.

QCM was first used in vacuum and in gaseous environments. However, Nomura showed that the piezoelectric crystal completely immersed in liquid can also oscillate in a stable manner [18]. This approch paved the way for many different applications, specially as a sensor in biomedical sciences.

The common electrical equivalence, Butterworth van Dyke (BVD) electrical model, for a quartz crystal resonator is shown in Figure 2.11. This model is often used to represent the electrical behavior of a crystal resonator near series resonance.

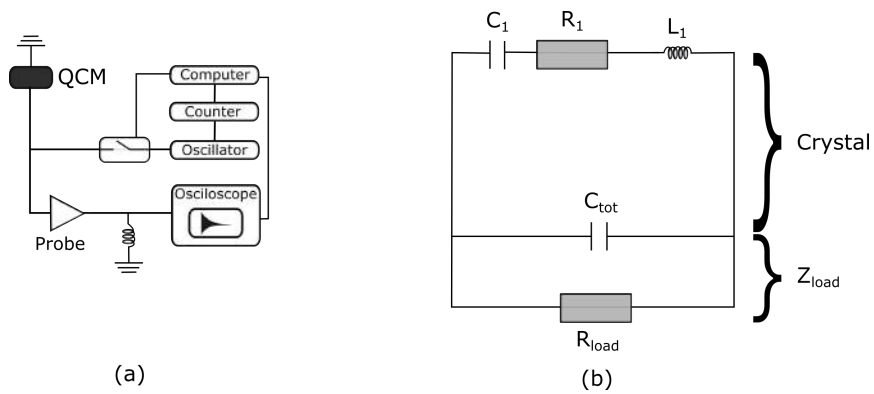

Figure 2.11: *Illustration of a QCM system (a) with the correspond eletric circuit (b).*

The BVD electrical model consists of two parts. On the top, the components are modified by the mass and viscous on the crystal: the resistor (R_1) is the

dissipation of the oscillation energy, C_1, the capacitor, corresponds to the stored energy in the oscillation and is related to the elasticity of the quartz and the surrounding medium and L_1, the inductor, corresponds to the inertial component of the oscillation. The second part has the componente C_{tot}, the parasitic capacitance, which represents the sum of the static capacitances and connector capacitance.

During a QCM measurement Δ_f is the indicator of mass, the frequency decreases as mass increase. It is also convenient to use the dissipation factor (D). In liquid, D increases due to viscous coupling.

The QCM operation in liquids is extremely sensitive to mass changes at the solid/solution interface. When QCM comes in contact with a solution, there is a decrease in frequency that is dependent on viscosity and density of the solution. The treatment of the influence of the solution on the crystal permits the prediction of the change in resonance frequency according to:

$$\Delta_f = -f_q^{3/2}(\frac{\rho_l \eta_l}{\pi \rho_q \mu_q})^{1/2} \tag{2.32}$$

where ρ_q and μ_q are the quartz density and shear modulus, respectively, η_l is the liquid viscosity and ρ_l is the liquid density. The f_q is the quartz resonator frequency. Δ_f and Δ_D measurements are both routinely used as independent indicators of mass loading and viscosity at the crystal-liquid interface.

2.4 Principles of Field-Effect Transistors

Field-effect transistors (FET) are semiconductor devices that can be used as potentiometric sensors since they are able to detect the eletric potencial change at the surface of a solid material when placed in contact with an electrolyte [19].

FETs has a basic structure of a metal-oxide-semiconductor field-effect transistor, or MOSFET. It consists of a p-type single crystal silicon semiconductor substrate with two heavily doped n-type regions (source and drain), a gate dielectric and a metal gate electrode on top of the gate dielectric. MOSFET has a high entrance impedance due to its insulate gate. The current flow between drain and source when a very small potential is applied to the gate terminal.

2.4.1 Extended Gate Field-Effect Transistor

In 1970, Bergveld introduced the ISFET (Ion Sensitive Field-Effect Transistor) [20] where the metal gate from the MOSFET is removed and the gate dielectric placed in contact with a liquid solution. The ions absorbed on the surface generates an electric field similar to applying a voltage at the metal gate. This devices were incorporated as pH-sensitive insulators or ion-selective membrane.

A new device was proposed in 1983 by Spiegel [21], the Extended Gate Field-Effect Transistor (EGFET). This FET has the sensitive part separated and coupled through a wire that is further attached to the transistor's gate. This new structure is easily constructed and does not require the fabrication of the MOSFET, being simple to produce. Other advantagen include that the field-effect electronic part does not enter in contact with the solution [21].

The physical principle involved on EGFET device is essentially potenciometric since the surface suffers a potentiometric change. The potential is directly driven to the MOSFET's gate through the extended gate wire and this potential controls the current flowing between Drain and Source terminals of the MOSFET.

To develop an EGFET device is necessary to link a sensible structure and an electronic component with a high entrance impedance. Figure 2.12a show the classical system where a commercial MOSFET is used and linked with the sensing structrure, that is inside a beaker, through the wire.

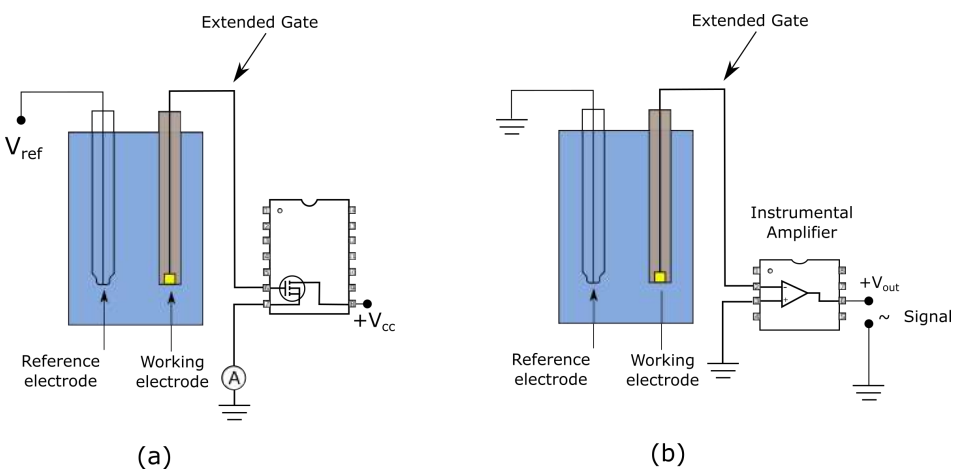

Figure 2.12: *Comparison between the classical EGFET system built with a MOSFET (a) and an anlternative EGFET systems built with an instrumental amplifier (b).*

It is also possible to use an instrumental amplifier as show in Figure 2.12b. In this case, the amplifier is set as unitary gain buffer. This modification reduces the hysterettic effect, reducing the input leakage and capacitance [21].

EGFET can be used for detection of charged biological species. When the gate is funcionalized with a biological recognition element, the FET is called BioFET. In this case, the change in the charge density of a biolayer immobilized on the gate induces a change in the electrode surface charge density, which in turn alters the surface potential and the BioFET acts as a potentiometric transducer [19].

The miniaturization and compatibility with microfabrication technologies make the BioFETs promising for the development of low-cost portable devices, especially for diagnosis.

Chapter 3

DNA Probe immobilization

Chapter 3 discusses the first challenge of this work: find the best protocol to develop a homogenous and stable self-assembled monolayer in order to have reproducible results. The electrode preparation protocol, sample preparation and different immobilization strategies are discussed.

3.1 DNA self-assembled monolayer

DNA hybridization sensors are based on DNA probes of known sequence immobilized on an electrode surface to detect a target DNA in solution. For the hybridization detection ocurs with success, the probe immobilization is the first crucial step in the sensor development.

Many efforts have been directed to develop different strategies to electrode surface modification. One of the most commonly strategies used involves the formation of self-assembled monolayers (SAM). The discovery of spontaneous alkenethiolate molecular film formation on gold [22] and the ability to form SAM on metal surfaces, initiated the research looking for different applications. Therefore, this modification consists in formation of a monomolecular layer with high organization that is spontaneously formed when the electrode is immersed in a solution composed of amphoteric molecules [23].

The SAM formation is based on the adsorption of functionalized alkanes on metallic surfaces. Thiols on gold surfaces are the most widely studied SAM type. It is characterized by perfect pairing between the alkanes with a slope of 20 to 30 degrees and in a high degree of organization and have been used in several

studies, including electron transfer, which is fundamental for the development of electrochemical sensors.[24]

Single-strand DNA (ssDNA) SAM use synthetic probes sequences modified with thiol group (Figure 3.1(a)) immobilized on gold surface through a sulfur-gold linkage. This design structure can exhibiting greater biological activity and selectivity once applied the correct protocol. For exemple, Herne and Tarlov [25] demonstrated that optimization of surface density of probes also depends on the ionic strength of the immobilization buffer. For hybridization sensors, the accessibility of immobilized probes to complementary target sequences can be enhanced by adding to the SAM a small molecule that work as a blocking agent and a spacer. 6-mercapto-1-hexanol, or MCH, commonly used. This small molecule can displaces the weaker adsorptive contacts between DNA nucleotides and the substrate due to thiol group, wich leads to a compact monolayer [26].

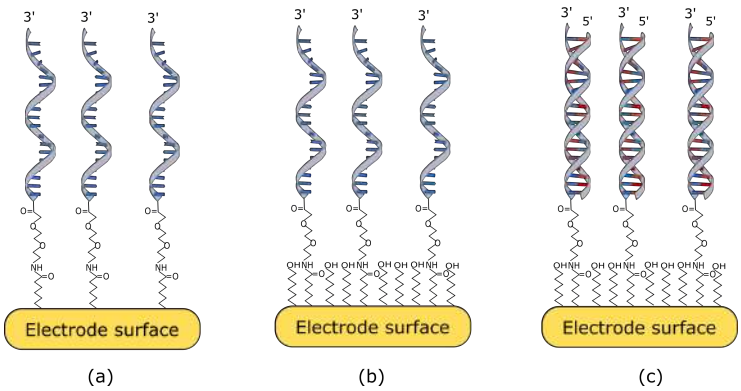

Figure 3.1: *Illustration of ssDNA immobilization on a gold surface (a), followed by a MCH immobilization (b) to built a self-assembled monolayer (SAM) and the hibridization event (c).*

The SAM configuration illustrated in Figure 3.1(b) presents a compact and organized layer where the spacer can effectively prevent the adsorption of hydrophobic DNA bases directly onto the gold surface, consequently, improving hybridization eficiency (Figure 3.1(c)) and reduces the non-specific adsorption of targets on the electrode surface.

Furthermore, the monolayer dimension (nanometers) avoids the slow diffusion of the electroactive species to the surface, reduces non-faradic residual currents, and also, promote the surface passivation once the accumulation of unwanted species on

the surface of the electrode is reduced.

3.2 Pretreatment of gold electrodes

Gold is an appropriate substrate for self-assembled monolayers, and the properties of this substrates play an important role on the formation of the SAM [23]. Gold substrate has a lot of advantages, but at the same time, is easily contaminated. This contamination can affect the SAM, creating defects that will dominate the electron transfer process, and consequently, affect the DNA hybridization detection. So, it is important to pretreat surface before.

Pretreatments can be divide between physical, chemical and electrochemical. Physical treatments involves mechanical polishing with different alumina particle sizes to remove a thin layer of gold and re-generate the surface of reusable electrodes. Chemical treatments are based on different methods to oxidize the surface, for example: piranha solution (a mixture of H_2SO_4 and H_2O_2), ozone or aqua regia . Cycling the electrode potential between limits at which the gold surface is oxidized and reduced is an effective electrochemical method to remove adsorbed impurities [27].

Generally, these different pretreatments can be combined to obtain a clean and reproducible surface roughness. Some studies [28, 29] reported that chemical cleanning, which leaves gold oxide on the surface, affect the SAM formation leading to non-reproducible results. As one of the main concern in this work is to obtain reproducible SAM, chemical methods as piranha will be avoided. Alternative procedures can combine physical and electrochemical methods.

3.2.1 Cleanning procedure

The final cleanning procedure presented in this section is an optimized pretreatment developed after different results obtained over the experiments. Polycrystalline gold working electrode (2mm diameter, 99.99%, Metrohm 6.1204.020, Switzerland) and a platinum counter-electrode (Metrohm, Switzerland) were used in all the experiments.

1. First the electrodes are electrochemically desorbed by scanning the potential

between -2.0 and -0.8 V (vs Hg/Hg_2SO_4) in a 0.5M NaOH solution. The negative potential reduce any remaining thiol groups adsorbed on the surface in previous experiments. Figure 3.2(a) shows the electrochemical dessorption highlighting the reduction peak of thiols.

2. Gold electrodes were polished using 1, 0.3 and 0.05 μm alumina particle size (Struers, Denmark) for 3 minutos each one. Between the polishes, the electrodes were sonicated in MilliQ water for 5 mins to remove alumina oxide particles residue.

3. Electrochemical cleaning by cycling from -0.5 V to 1.1 V (vs Hg/Hg_2SO_4) in 0.5 M H_2SO_4 for 50 cycles or until no change in the voltammograms. Figure 3.2(b) show the electrochemical cleaning voltammogram. The reduction peak and capacitive area are used to determine the surface roughness.

4. Finally, the electrodes are rinsed with MilliQ water, dry with nitrogen gas and immediately used.

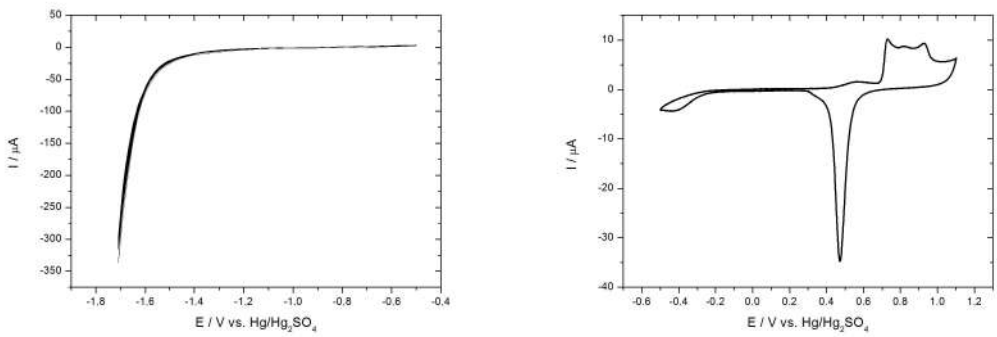

(a) (b)

Figure 3.2: *Cyclic voltammetry of the cleanning procedures. First, in (a), the dessorption in 0.5 NaOH follow by the eletrochemical cleanning (b) in 0.5 M H_2SO_4. Both using Hg/Hg_2SO_4 as reference electrode.*

3.2.2 Determination of the surface roughness

The properties of the gold electrode surface depends on the topography or roughness and chemical state. These factors affect the reproducibility, packing

density and ordering of the SAM. The pretreatment procedures presented above are able to remove organic impurities and reduces surface roughness.

Electrochemical cleanning, on step 3 above, repetitively oxidizes and reduces the gold surface in diluted acid and the voltammogram (Figure 3.2(b)) is used to determine the roughness factor (r). This factor is defined as the ratio between the real area (or microscopic area) and the geometric area (Area_G).

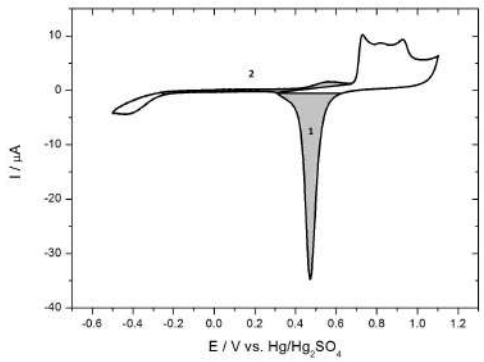

Figure 3.3: *Cyclic voltametry of the electrochemical cleanning procedure from -0.5 to 1.1 mV vs. Hg/Hg_2SO_4 in 0.5 M H_2SO_4. In gray, region 1 correspond to the capacitive area while region 2 correspond to the reduction peak. Both are used to determine the real surface area from an electrode.*

The reduction peak area represent the charge needed to reduce a monolayer of adsorbed oxygen on the gold surface in an anodic potential scan. Mathematically, the real area (Area_R) can be calculated by the area of the reduced peak subtracted from the capacitive area, both illustrated in Figure 3.3. The result is divided by the constant 390 μC/cm^2 for polycrystalline gold, as show in Eq. 3.1:

$$Area_R = \frac{1-2}{390} \tag{3.1}$$

$$r = \frac{Area_R}{Area_G} \tag{3.2}$$

where Area_G correspond in this case to π.radius^2 cm^2. The roughness factor was limited from 1 to 1.5 as acceptable values to use the electrodes in an experiment. The real areal is also used to normalize the electrochemical signals from each electrode.

3.3 Sample preparation

All reagents were obtained from Sigma-Aldrich and the solutions were prepared with MilliQ water (Millipore system) with a Biopak Polisher Ultrafilter (CDUFBI001) to remove pyrogen, nuclease and protease. DNA synthetic oligonucleotides were purchased from Sigma-Aldrich. The folowing sequences correspond to microRNAs related to breast and ovary cancer used in this study.

Table 3.1: *DNA sequences used in the work. The probe with thiol modification, the full complementary sequence (target), 4 mismatch and a non-complementary sequence. In red is highlighted the mismatch bases.*

Sample	Sequence
Probe (miR-200a)	5' -HS$(CH_2)_6$- TTTT ATTGTGACAGACCATTGCTACA-3'
Target (miR-200a)	3-TAACACTGTCTGGTAACGATGT-5'
4 mismatch (miR-200b)	3'-TAATACTGCCTGGTAATGATGA-5'
non-complementary (miR-200c)	3'-TAAACTGCCGGTAATGATGGA-5'

Note that in the sequence the bases U from RNA were replaced by T from DNA. This change gives the systems more stability and resistance against enzyme degradation. Indeed, these samples preparation need some care in order to maximize the shelf life.

3.3.1 Complementary sequences

All the complementary sequences are provided ready to use after resuspension. The sequences are resuspended adding TE buffer (10mM Tris e 1mM de EDTA), pH 7.5 with 100μM of stock solution. The samples are divided and maintained at -20°C.

3.3.2 Thiol-modified probe

Thiol-modified oligos are provided in protected form with disulfide bonding to minimize the oxidation potential. Sigma-Aldrich recommend to reduce the disulfide

bond with DTT in order to have a free thiol bond (-SH). DTT structure is illutrate in Figure 3.4.

To activate the thiol modification, 100mM DTT in sodium phosphate buffer, at pH 8.5, was added in the ependorf and kept at room temperature for 1 hour. After that, to remove the DTT, the sample was eluted in a NAP-10 column (GE Healthcare Life Science) with 50mM sodium phosphate buffer. The column should completely remove the DTT in the sample. However, after non-reproducible results was suggested that the DTT could still be in the probe sample, affecting the SAM formation.

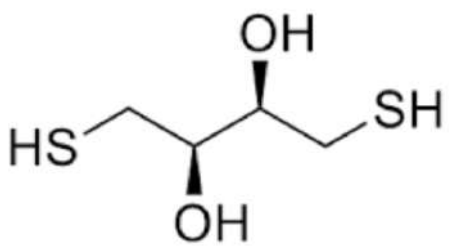

Figure 3.4: *Ditiotreitol (DTT) structure illustration.*

To elucidate this hypothesis a mass spectrometry was performed. MSMS m/z 177 shown in Figure 3.5 is the ion that was selected for fragmentation while the m/z is the mass to charge ratio used in the analysis of DTT. The molecular weight of this compound correspond to 154 g/mol. However, in solution, DTT can get charged or associated with other elements. One strong suggestion is the DTT association with sodium, which confers 177g/mol, as a high intensity peak in the spectrum.

The others less intensity peaks correspond to the possible breaks in DTT, as an example the second high intensity peak, 149.1 g/mol, may correspond to the loss of two CH_2. Figure 3.7 shows the electrospray ionization (EIS) positive of a ssDNA sample prepared using DTT where the 177 g/mol is present. So, it's possible to confirm that even using the elution column DTT is not completely removed from the samples interfering in the SAM formation.

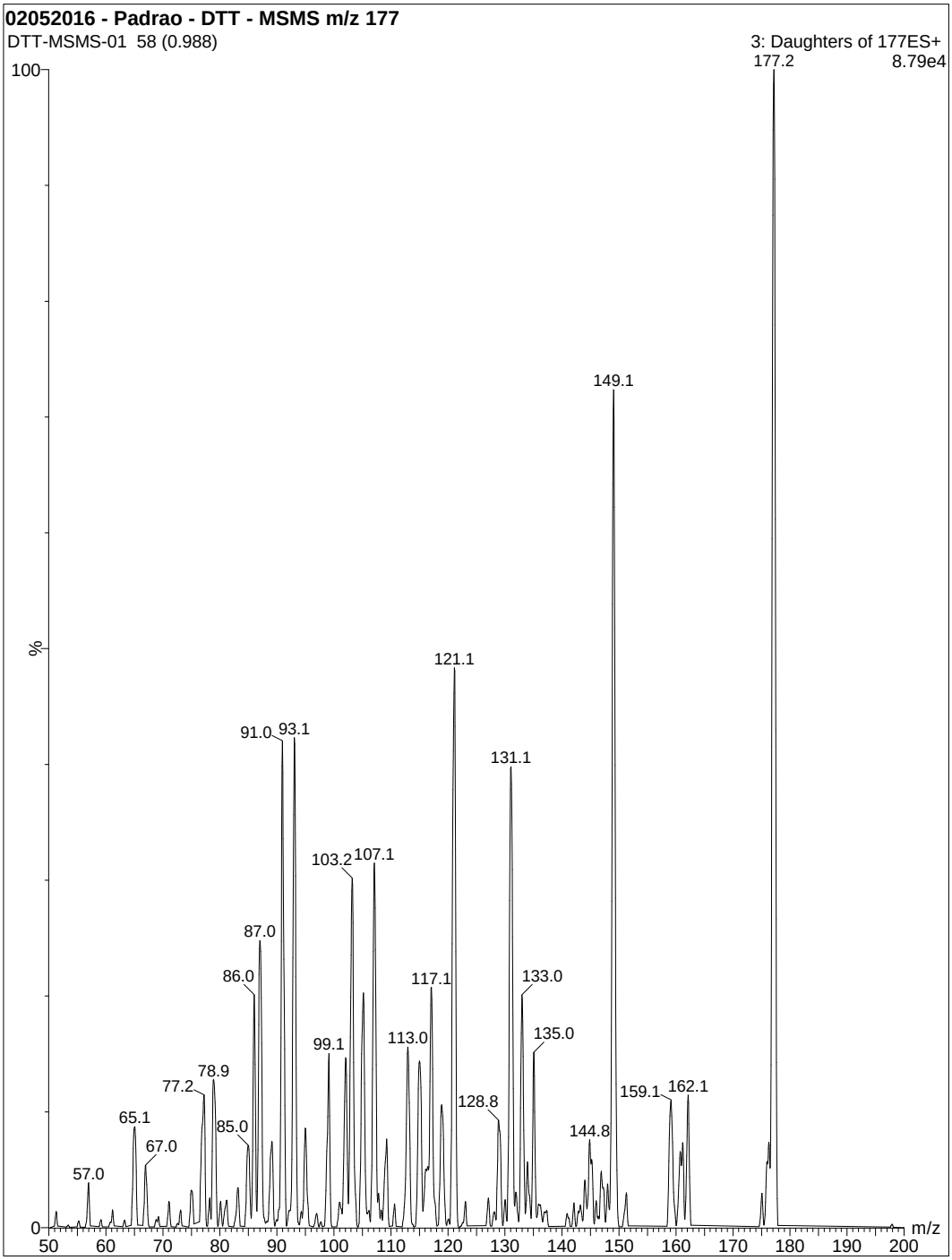

Figure 3.5: *MSMS m/z 177 is the ion that was selected for fragmentation while the m/z is the mass to charge ratio used in the analysis of DTT.*

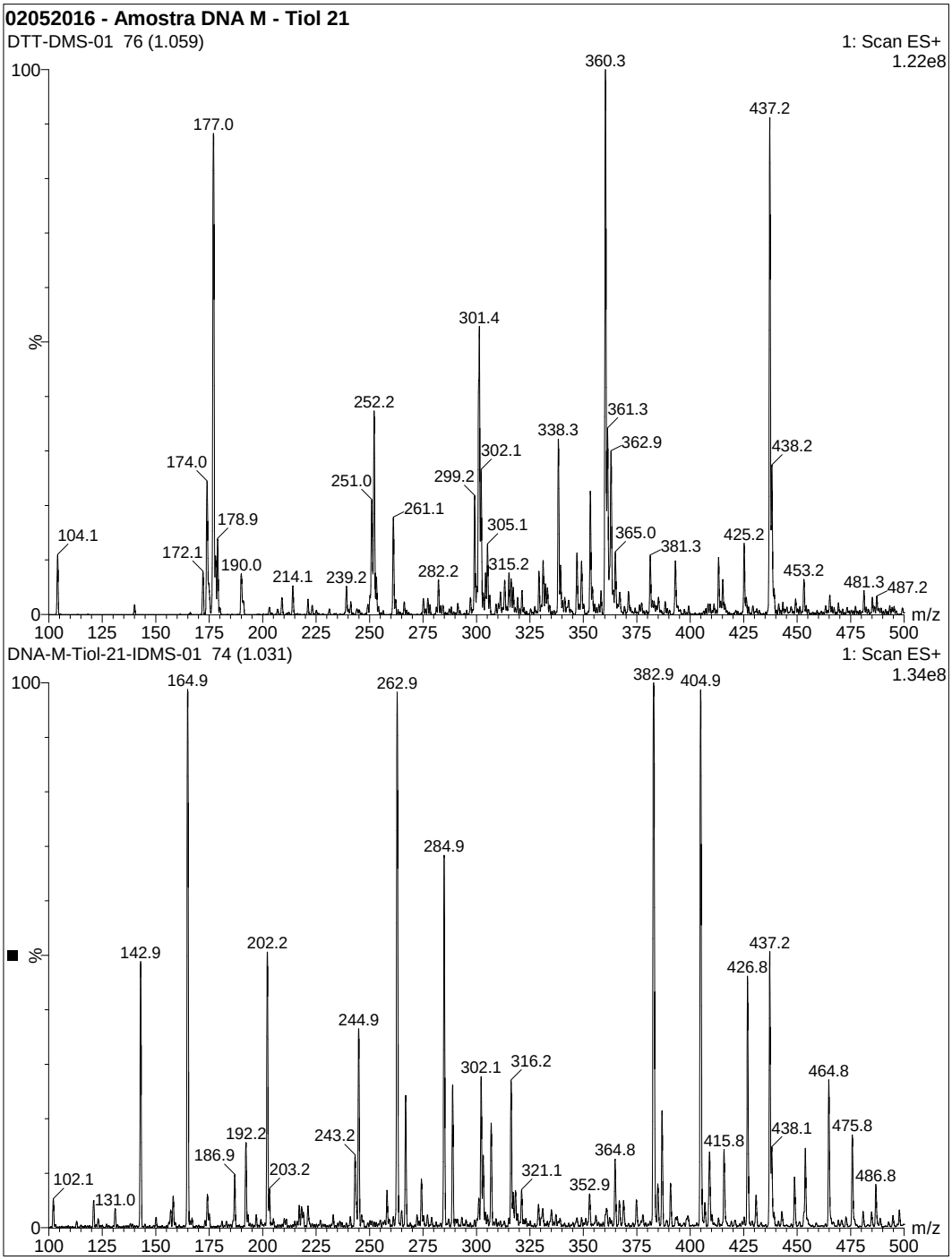

Figure 3.6: *Electrospray ionization (ESI) positive of a ssDNA sample prepared using DTT where the 177 g/mol is present*

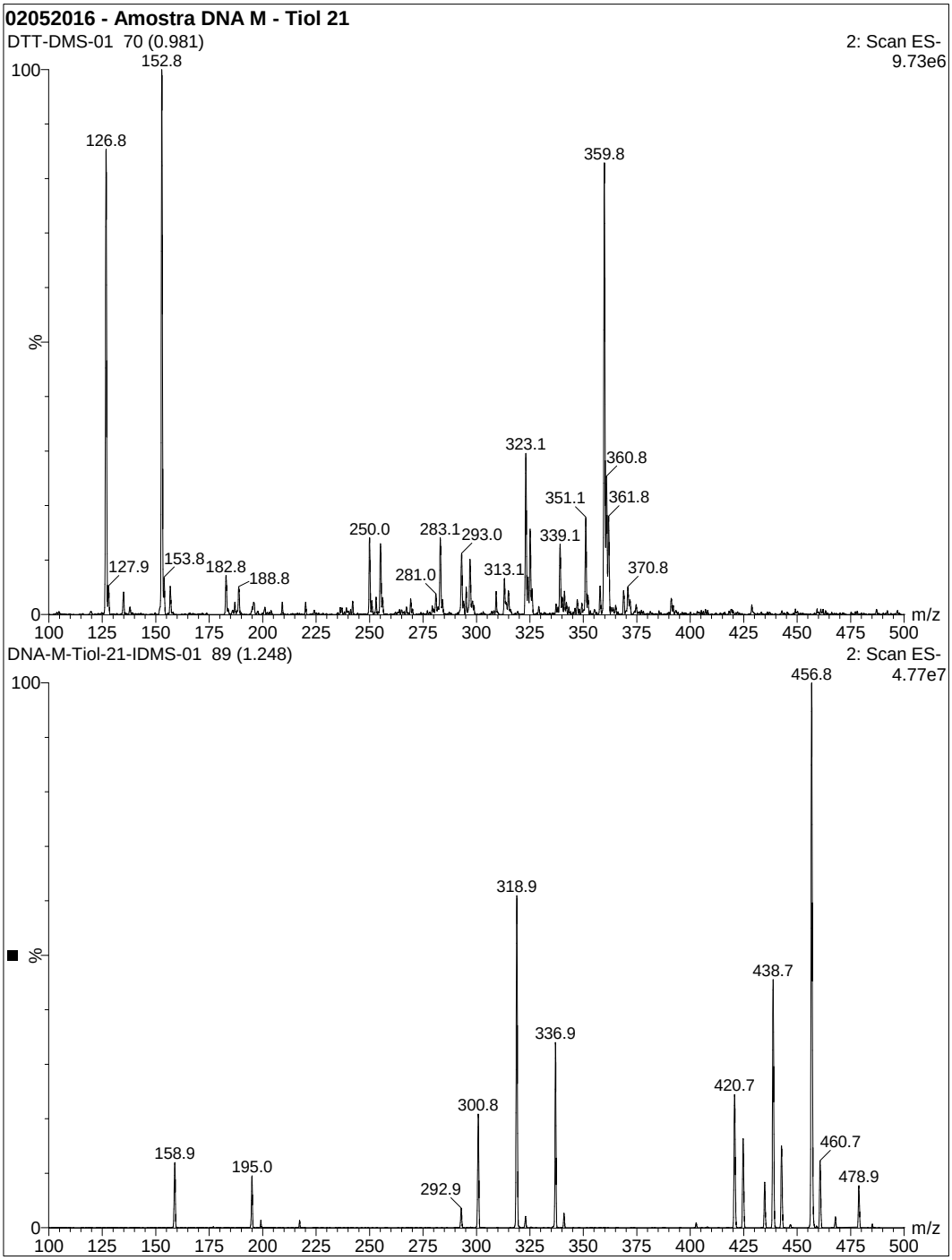

Figure 3.7: *Electrospray ionization (ESI) negative of a ssDNA sample prepared using DTT where the 177 g/mol is present*

3.4 DNA probe immobilization strategies

In the last decade many procedures describing the oligo probe immobilization have been reported. As mentioned before, the probe immobilization is the key step to the hybridization sensor once the interactions with the target sequence occur in a heterogenous surface. Therefore, first the immobilization method was optimized to produce a sensor surface with good control on the reproducibility.

Generally, the procedures have in commum the SAM formation, at room temperature, take from minutes to many hours, using different buffers with neutral pH and examined using different techniques to provide information on the electrode/SAM interface [23].

The following sections will discuss the immobilization strategies developed over this thesis. Briefly, the immobilization procedure can be divided in two groups: ssDNA immobilization followed by spacer immobilization or co-immobilization, where both species are immobilized at the same time. Apart from this, different buffers can be used. The first and second methods are based on probe immobilization followed by spacer, using a weak ionic strength immobilization buffer in the first, and a strong ionic strength buffer in the second. The third method use co-immobilization and a strong ionic strength immobilization buffer.

3.4.1 Weak ionic strength immobilization buffer

Literature describes different immobilization buffers for DNA hybridization sensors. Most of them are composed of Tris, sodium or potassium phophate buffer (PB) with NaCl (sodium chloride) and EDTA (Ethylenediaminetetraacetic acid), pH 7 - 7.5.

The first procedure started with 1μM ssDNA probes in TE buffer (described above) for 18 hours. The surface is washed with 10 mM NaCl in 5 mM Tris pH 7.4. After that, the electrodes are exposed to 1 mM MCH (in MilliQ water) for 2 h and washed again with 10 mM NaCl in 5mM Tris. The hybridization occurs with 1 μM target sequence in TE buffer for 1h. The electrochemical characterization was performed with 2.5 mM hexacyanoferrate II and III (1:1) in 10 mM Tris pH 7.4

Figure 3.8 shows the cyclic voltammogram(a) and the EIS (b) results of

this protocol. The voltammogram presents a resistive and irreversible profile for ssDNA before and after the spacer MCH. Likewise, EIS does not provide a half-circumference as response.

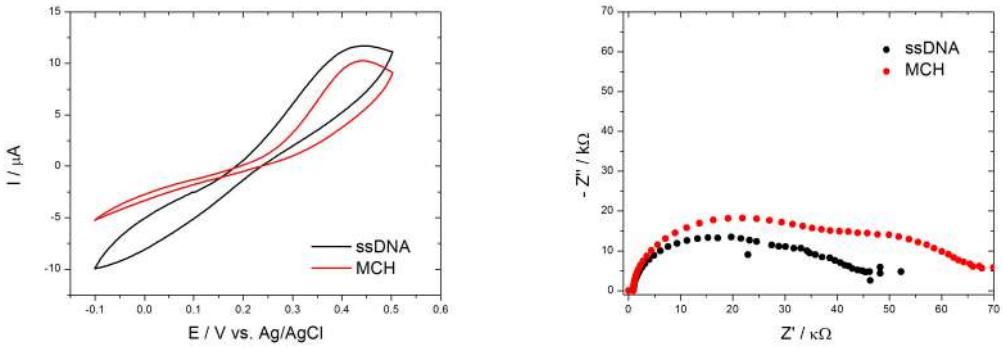

(a) (b)

Figure 3.8: *Cyclic voltammetry (a) and electrochemical impedance spectroscopy (b) (vs. AgAgCl) for probe immobilization (black) followed by MCH immobilization (red) to block the surface avoiding non specific interaction. Both using 2.5 mM hexacyanoferrate II and III (1:1) in 10 mM Tris, pH 7.4, 100 mV/s*

It was already reported that the surface density of the probe depends on the ionic strength of the immobilization buffer [25]. The ionic strength can screen the DNA charge to allow high probe densities. In this case, TE buffer used for immobilization has a low ionic strength, which reduces the probe densities and the ssDNA can flat on the electrode surface, blocking it. Once it happens, MCH may not be enough to remove all non-specifically adsorbed probe from the surface [30]. As a result, a non-compacted SAM is formed.

3.4.2 Strong ionic strength immobilization buffer

To improve the electrochemical signal from the DNA hybridization sensor other reagents were added to the immobilization and hibridization buffers. In the second procedure tested the immobilization buffer was replaced by 1 M potassium phophate buffer, pH 7, where 1 μM ssDNA where diluted and kept 18 hours at room temperature. After that, the electrodes were exposed to 1 mM MCH (in MilliQ water) for 1 h and washed with 10 mM NaCl in 5 mM PB, pH 7.4. The hibridization of 1 μM tDNA occured in 1 M NaCl, 1mM EDTA and 10 mM PB, pH

7.4, in 1 h. The CV and EIS were performed in 2.5 mM hexacyanoferrate II and III (1:1) in 10 mM PB, pH 7.4.

Potassium phophate buffer was tested as immobilization buffer in a high concentration. The EDTA, now into the hybridization solution, is known as a chelating agent that has high affinity for ions, mainly cations with +2 and +3 charge. It is widely applied for biological purposes, mainly to avoid DNA degradation [31]. As DNA has negative charge due to phosphates groups it is interresting to add a positive charge as Na+, from NaCl, on the hibridization buffer to promote the neutralization of these charges.

The electrochemical characterization of this procedure is presented in Figure 3.9. In the voltammogram, on the left, and in the EIS, on the right, the three curves correspond to the ssDNA immobilized (in black), the surface blocked with MCH (in red) and the hibridization with 1μM of target DNA (in blue).

By blocking part of the gold surface with the ssDNA an initial resistance arises. This resistance can be interpreted as the resistance to the charge transfer between the electrode surface and the redox marker in solution. When MCH is added it increases the surface block, increasing the resistance proportionally to the number of species adhered. Hybridization, on the other hand, is responsible for changing the DNA conformation and its mobility, making it more rigid. It also interferes in the charge transfer, increasing it. Both responses are observed in the voltammogram and the impedance spectra.

The displacement of the oxidation to more positive values and reduction peaks to more negative values, in Figure 3.9(a), indicates the surface blocking. The hybridization was able to be detected, but its displacement, in relation to the previous curve, was significantly lower. Table 3.3 shows the information extracted from the voltammogram.

From EIS, in Figure 3.9(b), it is possible to observe the charge transfer resistance (R_{ct}) from the half-circumference of the Nyquist diagram and the values are described on Table 3.3. R_{ct} from a clean electrode correspond to 300 Ω. With ssDNA immobilization this value increased to 5.01 kΩ. When the surface is blocked with the spacer, R_{ct} increases to 27.86 $k\Omega$ and the hidridization correspond to 42.62 $k\Omega$.

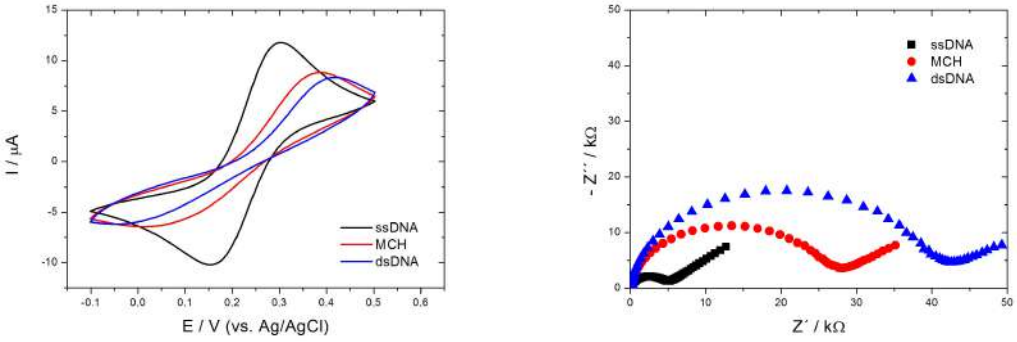

(a) (b)

Figure 3.9: *Cyclic voltammetry (a) and electrochemical impedance spectroscopy (b) (vs. Ag/AgCl) for probe immobilization (black) follow by MCH immobilization (red) and hybridization with 1µM target DNA. Both using 2.5 mM hexacyanoferrate II and III (1:1) in 10 mM PB, pH 7.4, 100 mV/s*

Table 3.2: *From the voltammogram in Figure 3.9(a) it is possible to extract the potentials of the anodic and cathodic peak. Also, the difference betwenn them, ΔE, for each step of the immobilization and hybridizaiton.*

Step	E_{pa} (V)	E_{pc} (V)	ΔE (V)
ssDNA	0.30 ± 0.01	0.15 ± 0.01	0.15 ± 0.02
MCH	0.38 ± 0.02	-0.04 ± 0.01	0.42 ± 0.16
tDNA	0.41 ± 0.02	-0.04± 0.03	0.45 ± 0.04

Table 3.3: *The main information extracted from EIS (Figure 3.9(b)) is the charge transfer resistance (R_{ct}). This value is show for each step for, at least, three different electrodes.*

	ssDNA	MCH	dsDNA
R_{ct} (kΩ)	5.01 ± 1.10	27.86 ± 11.14	42.62 ±11.91

The second procedure demostrates the importance of NaCl and EDTA in the formation of the monolayer. Using EIS, it is observed 71.44% R_{ct} increase with 1μM tDNA. This concentration is described in the literature as sufficient to hybridize all the ssDNA immobilized [5]. The limit of detection (LOD) of the hybridization correspond to the lowest analyte concentration likely to be reliably distinguished

from the monolayer and at which detection is feasible. It can be determined by an analytical curve decreasing the concentration of the target DNA in solution until no charges are detected.

Figure 3.10 shows the CV (a) and EIS (b) results for ssDNA, MCH and different tDNA concentrations. In (a) the distance between the oxidation and reduction peaks increase with the increasing tDNA concentrations. In (b) R_{ct} increases from 4.7 kΩ with MCH to 13 kΩ with 1 μM.

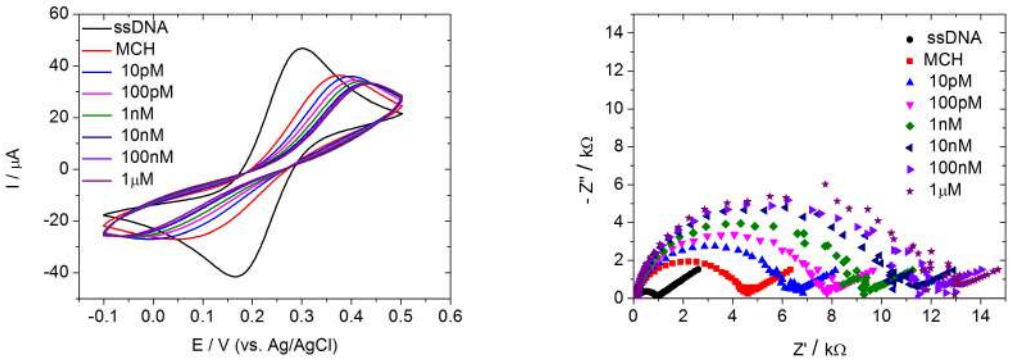

(a) (b)

Figure 3.10: *The ssDNA immobilization follow by MCH immobilization is tested over different target DNA concentrations. The CV in (a) shown a shift in the peaks with the target DNA increase while the EIS (b) shown a increase in the R_{ct} in the same conditions.*

The impedance spectra gives a linear R_{ct} increase as a function of tDNA concentrations, as show in the analitical curve in Figure 3.11.

However, despite the apparent success of this immobilization method, the electrochemical characteristics were not reproducible. This suggests that this low reproducibility was caused by a non-compact SAM, where the ssDNA interact with the gold surface and the post-immobilization treatment with MCH were not enough to remove all non-specifically adsorbed probe [30]. At the same time, the immobilization buffer with PB was not able to promote a SAM formation with high probe density.

3.4.3 Co-immobilization with a strong ionic strength buffer

Finally, the third strategy applied is based on the mixed SAM structure proposed by Herne and Tarlov [25], where they demonstrated that the density of

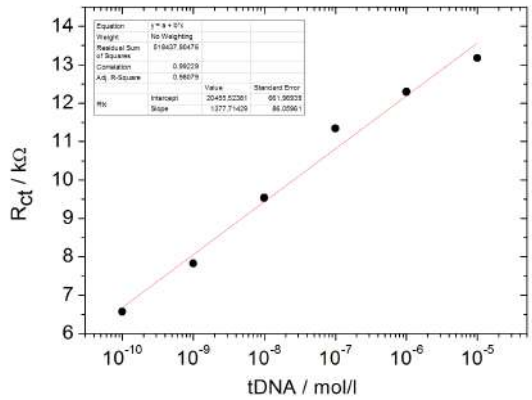

Figure 3.11: *The R_{ct} values from the Figure 3.10(b) are presented a linear behavier when the concentration of target DNA increase.*

probes strongly depends on the ionic strength of the immobilization buffer. They also confirmed that the adsorption of DNA bases on gold, especially the interaction of base A with gold, is so strong that it can dehybridize duplex sequences with this base, which results in low stability.

In this method the thiol modified probes are co-immobilized with a the same spacer, MCH. The new SAM prevent the adsorption of DNA bases directly onto the gold surface, improving hybridization efficiency and reducing the non-specific adsorption of targets [32].

Considering molecular size thickness of the SAM and the substrate is not completely flat, the defects in the monolayer are inevitable. These defects, as holes for example, may have a significant effect on the electrochemical behavior. The protocol to prepare a mixed SAM structure was also reported by Estrela adding a backfilling step [5]. After the SAM formation, the electrode is exposed to a high concentrate MCH solution to cover any remaining hole. The improved protocol proved to have a better control of probe density and good reproducibility [5].

The final method tested to DNA probe immobilization and followed over the thesis is based on the report above. The procedures, results and discussion will be shown in details in the next chapter.

Chapter 4

DNA hybridization detection

The use of the intrinsic negative charge from the phosphate backbone of DNA molecules is the base for hybridization detection and has achieved considerable interest [3]. Hybridization results in an increase of negative charge at a funcionalized surface probe and change the interface potential [5]. This change in potencial can be transduced using different potentiometric techiniques, including Electrochemical Impedance Spectroscopy (EIS) [5] and Field Effect Transistors (FET) [33].

One of the main advantages of these techniques is that they are promissing for label-free detection. EIS measures the charge transfer resistance (R_{ct}) in the presence of a negatively charge redox couple, in this case ferri/ferrocyanide in solution. Hybridization increases the negative charge on the electrode interface, but also, increases the repulsion for the negatively charged redox couple, increasing R_{ct} [34].

FETs can also be used to transduce when the system has a shift in the current-voltage characteristics. The devices are built with different designs based on funcionalization of the gate, which gives them different names as ISFET or EGFET. In the EGFET system, the extended gate allows to connect thin films modified with polymers and biomolecules [35]. Both techniques gives important information about the detection. However QCM also give information in real time about the SAM immobilization as the detection dynamics.

The third immobilization method discussed in chapter 3 is used in this chapter to develop the DNA hybridization sensor. Electrochemical detection with the presence of redox marker in solution is investigated. Probe surface density is controlled by the thiol molar ratio in solution and determined using

chronocoulometry. The limit of detection without further amplification is determined and the non-complementary sequences of microRNA 200b and 200c are tested. The same system is tested using QCM and FET detection to compare with EIS signal.

4.1 MicroRNA

MicroRNAs (miRNA) have emerged as a new class of biomarker with potential to be applied in the next generation of cancer therapeutics [36]. They are defined as a class of non-protein-coding and small RNAs (12 - 25-mer). Since their discovery in 1993 [37], these RNAs have been shown to play important regulatory roles in different gene expression and cellular processes [36].

Between all the cellular processes some studies show that specific miRNAs regulate cell proliferation and apoptosis processes, which are important in cancer formation. Though different molecular techniques, it was possible to determine that more than 50% of miRNA genes are located in cancer-associated genomic regions. Thus suggesting that they may play a more important role in human cancers than previously thought [38].

In a few words, these non-coding RNAs are divided into ribosomal RNA (rRNA), transfer RNAs (tRNA), nuclear RNAs (snRNAs) and nucleolar RNAs (snoRNAs). They also are subdivided into short and long non-coding RNAs (more than 200-mer). Long non-coding RNAs are particularly well suited to epigenetic regulation once they bind to complementary target sequences in the genome. After binding to their genome targets, they help recruit proteins that modify chromatin [39].

Short non-coding RNAs (including microRNAs) work by binding to target mRNA, where they can repress translation or cause the target degradation, as briefly illustrated in Figure 4.1. As consequence, miRNAs reduce the amount of protein produced by an mRNA.

MicroRNAs can be detected in blood and urine [39] providing the possibility for the development of new biosensing technologies based on oligonucleotides that are complementary miRNAs associated with disease and useful biomarkers for cancer

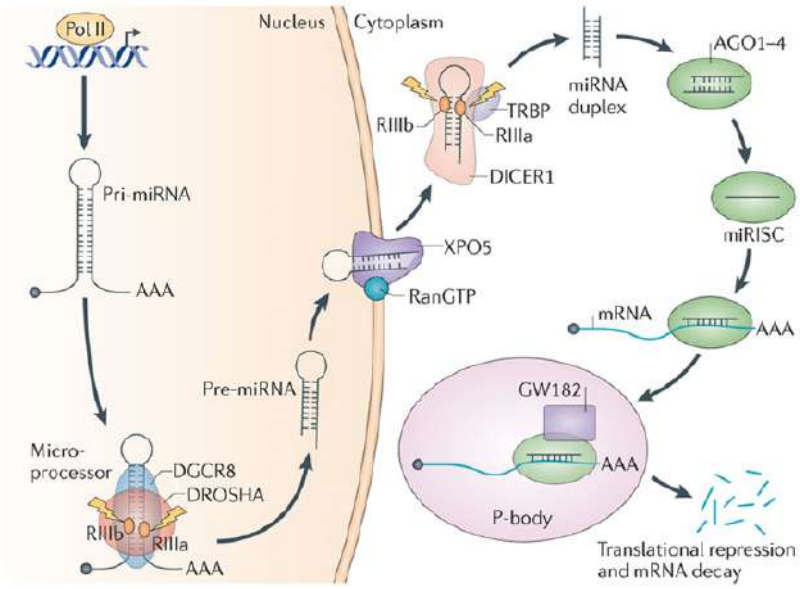

Figure 4.1: *The MicroRNA biogenesis process begins in the nucleus where the RNase III enzyme Drosha, coupled with its binding partner DGCR8, cleaves pri-miRNA into pre-miRNA. Pre-miRNAs are exported from the nucleus into the cytoplasm, where the hairpin precursors are cleaved and its binding partner the transactivator RNA-binding protein TRBP into dsRNA duplex that contains both the miRNA strand and its complementary strand. Reproduced from [39].*

diagnostics.

For this work the miR-200a was chosen as the probe for biosensor development. The sequence was tested with its full complementary or target, and also with miR-200b and miR-200c. These microRNAs are involved with ovarian and breast cancer [40]. In ovarian cancer these three sequences are overexpressed and miR-200a plays an important role in breast cancer initiation and progression.

4.2 Biosensor Fabrication

4.2.1 Materials

All DNA sequences were purchase from Sigma-Aldrich. All chemical used in the experiments were also purchased from Sigma-Aldrich and used as received. The aqueous solutions were prepared using Ultra-pure water (Millipore) with a Biopak Polisher Ultrafilter (CDUFBI001) filter to remove pyrogen, nuclease and protease and filter with 0.22 μm syringe filter before using.

4.2.2 Sample preparation

Thiol-modified probe and complementary sequencies were prepared using TE buffer adding a specific volume to obtain 100 μM. The samples are divided in small aliquots and frozen at - 20 ^{o}C until use. The sequences were previously described in Table 3.1.

4.2.3 Electrode preparation

Electrode preparation is based on the cleanning procedure described on section 3.2.1. Briefly, the electrodes are scanning to negative potential to remove thiol adsorbed groups in the surface. After that, the electrodes are polished with different alumina particle sizes, washed and electrochemically cleanned in sulfuric acid. Electrodes are rinsed in water, dried in steam of nitrogen and immediately exposed to ssDNA with MCH in the immobilization buffer.

MCH is first diluted in ethanol (BioUltra) (100 mM) and then, rediluted in water (10%) to obtain 1 mM. DNA immobilization buffer (I-BFR) consisted of 0.8 M phosphate buffer (PB) + 1.0 M NaCl + 5 mM $MgCl_2$ + 1 EDTA, pH 7.0. ssDNA and MCH were co-immobilized in different molar ratios to optimize the probe surface density, for 16 h at 4 ^{o}C.

After immobilization, electrodes were sequentially rinsed in I-BFR followed by 200mM PB, 10mM PB + 10mM EDTA and finally 10mM PB to remove any remaining Mg^{2+}. To ensure the complete thiol coverage of the gold surface, the electrodes were backfilled with 1 mM MCH (10%) immersion for 1 h at room temperature. Electrodes were finally rinsed with water.

All the electrochemical characterization was performed in 2.5 mM ferri/ferrocyanide in 50 mM PB + 100 mM K_2SO_4, pH 7.0 (E-BFR). Hybridization were performed using different complementary sequencies in 50 mM PB + 100 mM K_2SO_4, pH 7.0 (H-BFR) for 30 min.

4.2.4 Instrumentation

All electrochemical characterizations were carried out in an electrochemical cell with the 3 electrodes configuration, using a $Hg/HgSO_4$ electrode (FATEC) as

the reference electrode and a platinum wire as the counter electrode (Metrohm). An Autolab PGSTAT20 (Metrohm) was used to perform the electrochemical experiments with a FRA module.

4.3 Electrochemical characterization of modified electrodes

Once the protocol for ssDNA immobilization is well defined and the results in a compact and reproducible monolayer, it is importante to have an accurate control of probe density to optimize it and improve the hybridization signal. Now, the SAM is formed by a simultaneous co-immobilization of thiol-modified ssDNA and a thiol spacer MCH. So, first, the probe density is investigated through chronocoulometry (CC) and EIS.

4.3.1 DNA surface density

The ssDNA density on the SAM can be quantified with the chronocoulometry (CC) method developed by Steel et al. [26]. The electrodes modified with SAM are immersed in 10 mM tris buffer, pH 7.4. The potential is stepped from - 300 to - 800mV (vs. $Hg/HgSO_4$) for 500 ms to determine the capacitive charge. After that, the eletrodes are immersed in 100 μM hexaammineruthenium(III) chloride ($Ru(NH_3)_6{}^{3+}$) in Tris buffer and the measurement repeated. Both solutions used were purged with argon for 30 min before the experiments.

The positively charged $Ru(NH_3)_6{}^{3+}$, in this case, interacts electrochemically with the negatively charged probe being trapped stoichiometrically (1/3) to the amount of DNA bases [25]. To optimize the detection, different molar ration between thiol-modified ssDNA and MCH or the total thiol (ssDNA + MCH) varied from zero, where only MCH was immobilized, to 100% that corresponds to just ssDNA on the surface. The typical chronocoulometric curve for ssDNA with and without $Ru(NH_3)_6{}^{3+}$ and the hybridization with $Ru(NH_3)_6{}^{3+}$ is presented in Figure 4.2.

From the CC curve it is possible to extrapolate the ssDNA dada without $Ru(NH_3)_6{}^{3+}$ to y-intercept which corresponds to capacitive charge (Q_{dl}). Likewise, the ssDNA with $Ru(NH_3)_6{}^{3+}$ extrapolation correspond to the sum of $Q_{dl} + n_e A\Gamma_0$,

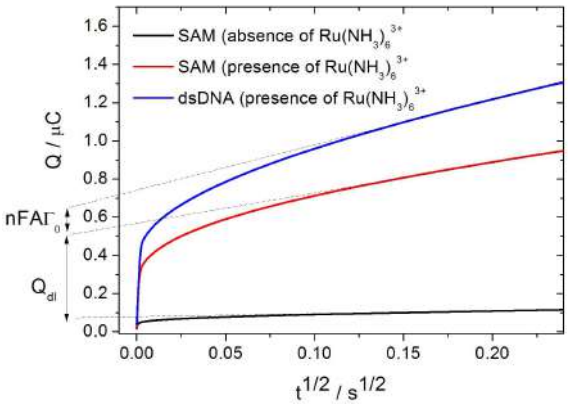

Figure 4.2: *Chronocoulometric response curves for DNA probe co-immobilized with MCH. In black the SAM in the absence of $Ru(NH_3)_6{}^{3+}$, in red the SAM in the presence of the complex and in blue, after hybridization with 1μM of target DNA and in the presence of $Ru(NH_3)_6{}^{3+}$.*

the charge from the reduction of Γ_0, the amount of surface confined redox marker (mol/cm^2).

Figure 4.3(a) show the CC curve for ssDNA in the molar ratio: 0, 1:10, 1:6, 1:5, 1:4, 1:3, 1:2 and 1:1 DNA:total thiol. The EIS curve for the same proportions are show in (b). The probe surface density varies from 2.84 .10^{12} cm^{-2} at 10% fraction of ssDNA to 9.47 .10^{12} cm^{-2} at 50%, while the R_{ct} varies from 5.1 to 12.2 kΩ at the same fractions.

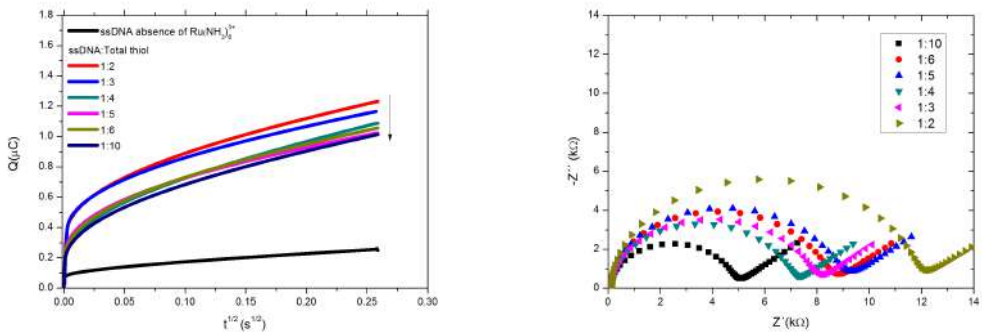

(a) (b)

Figure 4.3: *Electrochemical characterization of the SAM using different proportions of probe and spacer. Chronocoulometric response curves in (a) show the SAM in the absence of $Ru(NH_3)_6{}^{3+}$ in black and the different proportions with the presence of the complex. In (b) the EIS response curves in 2.5 mM ferri/ferro in E-BFR at OCP value.*

The Γ_0 values are describe in Table 4.1. Error bar show the spread for at least three electrodes at each molar fraction.

Table 4.1: *ssDNA surface density and charge transfer resistance values are presented for each probe and spacer proportion tested.*

DNA:Total thiol	Γ_0 (10^{12} cm^{-2})
0	2.30 ± 0.23
1:10	2.84 ± 0.24
1:6	3.27 ± 0.36
1:5	3.26 ± 0.34
1:4	3.61 ± 0.28
1:3	3.78 ± 0.48
1:2	4.31 ± 0.24
1:1	9.47 ± 1.18

The ssDNA surface density as a function of the molar ratio in the immobilization solution is show in Figure 4.4. Zero DNA/Total thiol correspond to the electrode immobilized with MCH. The fractions 1:10 and 1:6 (correspond to 0.1 and 0.16) show a small variability between electrodes in the same molar fration. It may be related to the decrease of electrostatic repulsion between probes. It, also, presented a linear relation between 10 and 50%.

High density values are interesting for DNA hybridization sensors due to the high target hybridization that can be obtained. This method has already been reported to investigate probe density by Steel *et al.* and Keighley*et al.* [26, 5] using different sequences, linkers and immobilization methods. The first one reported the high hybridization efficiency for the 4 x 10^{12} cm^{-2}, while the second one reported the maximum change in R_{ct} with around a 20% molar fraction (1:5), which correspond to, in this case, 5.4 x 10^{12} cm^{-2}.

The hybridization efficiency was tested with 1 μM fully complementary DNA in E-BFR for 30min. The result as a function of probe density is shown in Figure 4.5 and as a function of molar fraction in Figure 4.6.

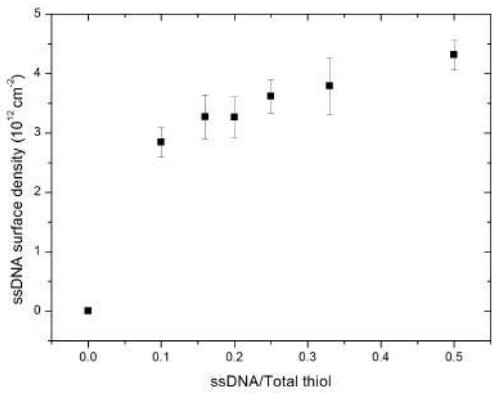

Figure 4.4: *Probe surface density as a function of fraction of DNA to total thiol concentration in immobilization solution. Error bars show the mean and spread for, at least, three samples at each DNA mole fraction.*

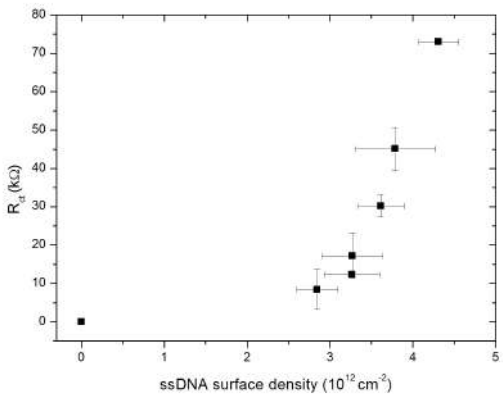

Figure 4.5: *Charge tranfer resistance (R_{ct}) as a function of probe surface density. EIS measurements are preformed in E-BFR with 2.5 mM ferri/ferro at OCP value.*

The R_{ct} from ssDNA SAM changes according to the ssDNA molar ratio as described in Figure 4.3(b). So, the R_{ct} after hybridization considering this change in shown in Figure 4.6. The maximum change in R_{ct} after hybridization occurs around a 20% fraction of DNA/total thiol in the I-BFR, which corresponds to 1:4 sample. This molar fraction is close to the reported by Keighley*et al.*, where the immobilization method is based. However, Keighley*et al.* used a ssDNA sequence with a different and longer linkers.

Considering these parameters optimized, the molar fraction 1:4 is tested over lower tDNA concentrations. The electrode was sequentially exposed from 10 fM to

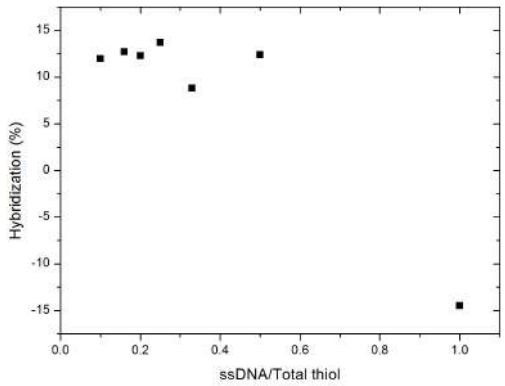

Figure 4.6: *Increase in the charge tranfer resistance (R_{ct}) after hybridization as a function of the fraction of DNA to total thiol. EIS measurements after hybridization are preformed in E-BFR with 2.5 mM ferri/ferro at OCP value.*

1μM for 30 min each. The analitical curve (Figure 4.7) shows the R_{ct} increase. From these values the LOD correspond to 100fM.

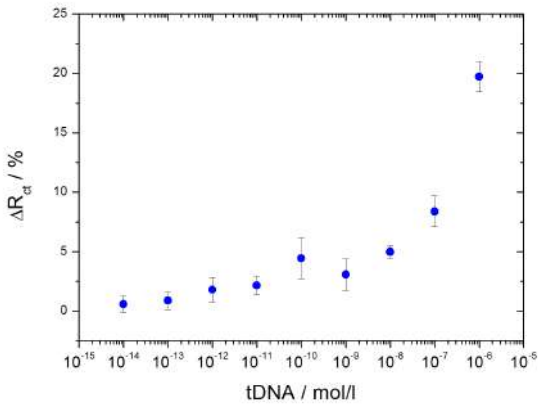

Figure 4.7: *Data points represent average R_{ct} recorded using EIS from four independent samples at different concentration of tDNA.*

The LOD is high compared to the current literature. However, this system does not have any signal amplification as nanoparticles, redox intercalators or probes without charge. Also important, Figure 4.8 presents the negative controls.

The electrodes are exposed to 1 μM miR-200b and 200c sequences for 30min. The R_{ct} for miR-200b with four mismatch, increased 2.4% while miR-200c, that is non-complementary sequence, show a small reduction.

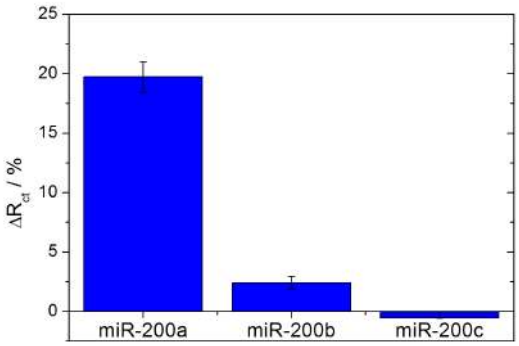

Figure 4.8: *The negative control. R_{ct} comparison between non-specific miR-200b and miR-200c sequences hybridization with miR-200a probe in the SAM.*

In this platform the hybridization efficiency was lower than previous results. However, the system has able to distinguish full complementary sequence from 4 mismatch bases and non-complementary sequences.

4.4 Hybridization Troubleshooting

4.4.1 Thermal Melt Analysis

The optimized DNA immobilization protocol described and discussed until this point ensure the best conditions for oligo immobilization on gold surfaces. However, once immobilized it does not ensure that the hibridization will successfully occur. The electrode surface hybridization could not occur for different and unknown reasons.

It is possible to test if the hybridization occurs in solution using a thermal melt analysis system. In this experiment, a Shimadzu UV-1800 spectrophotometer equipped with the TMSPC-8 was used for the thermal melt experiment. 1 μM concentration of DNA probe, target DNA and the mixture of probe and target DNA was prepared separately in E-BFR. The first cell is used to measure the blank with E-BFR followed by 2 cells for probe DNA, 2 cells for target DNA and 2 cells for mixture (probe + target) respectively. The programme is set with a complete cycle where the temperature is raised linearly from 19°C to 90°C and back. Using a ramp rate of 0.5^{o}C/min, the absorbance was recorded at a wavelength of 260 nm.

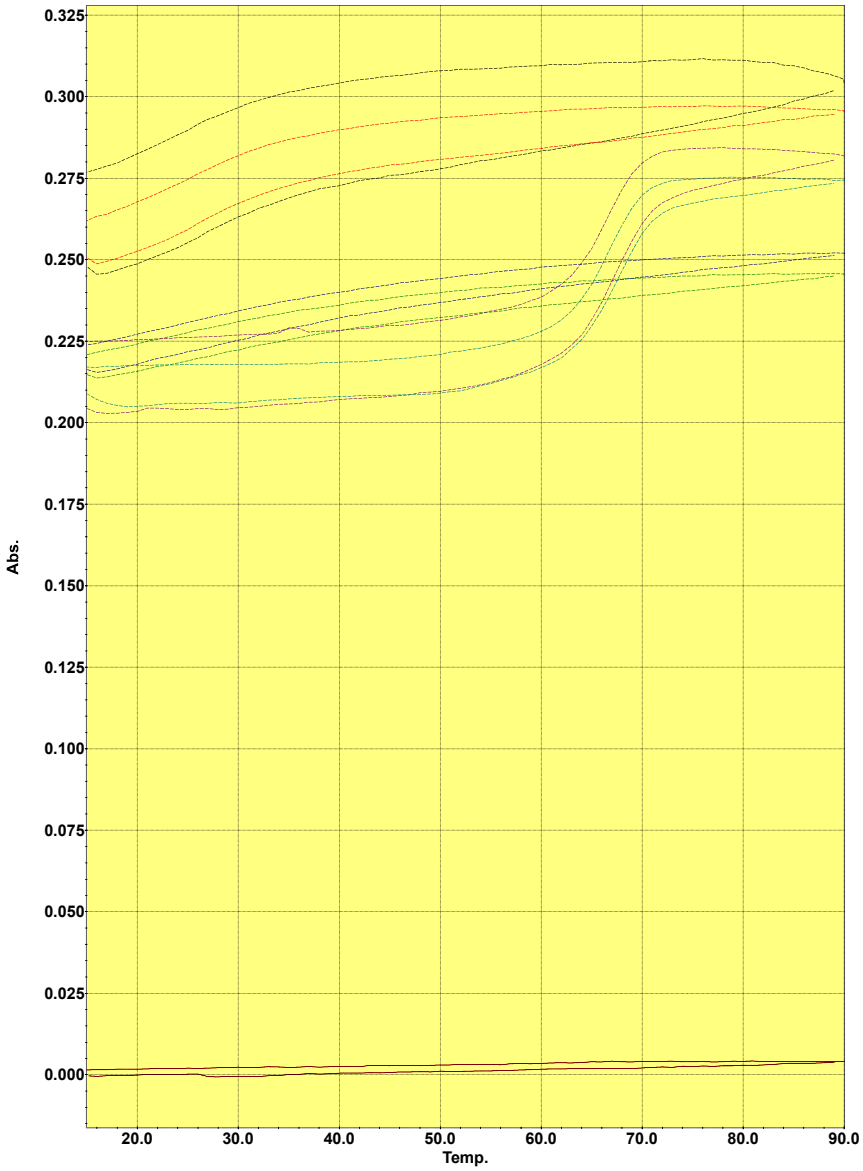

Figure 4.9: *Melting curve of DNA probe and target DNA in E-BFR buffer, pH 7.4. The zero absorbance correspond to the cell with E-BFR. The four different lines with a small increase over the temperature correspond to probes and targets in individual cells. The two curves with a significante increase around 66°C correspond to the cells with probe and target sequence together.*

Absorption can be used to detect the sample hybridization, in solution, as a function of temperature. Figure 4.9 demonstrated the real-time melting curve obtained. The DNA strands hybridize at room temperature and with the increase of temperature, the conformation changes until 60°C. Up to this value, the double helix denatures, increasing the absorbance. When the temperature decreases, the single strands hybridize again and the absorbance reduces. The temperature at which half of DNA strands are in the single-stranded state is termed as melting temperature (T_m). From the software analysis, the T_m was found to be 66°C. The analysis confirmed that the strands obtained were well hybridize even when it does not hibridize on the electrodes surface.

4.4.2 Linker

Oligo sequences are provided with different modification, as thiol or amine i.e., depending on the surface where it will be immobilized. Between the modification and the oligo sequence, there is a short structure, called linker. This struture normally depends on the company that it is synthetized. Some common linkers are $(CH_2)_6$, $(CH_2)_6$-PO_4-$(CH_2CH_2O)_6$ and AEEA(8-amino-3,6-dioxaoctanoic acid).

The linker increases the probe length and, also, can interfere in the electrostatic interaction between the probes on the electrode surface. A different linker is tested with the same DNA sequence to evaluate it's influence over the probe immobilization followed by hybridization. This part of the project was developed in the University of Bath (UK).

The HS-$(CH_2)_6$-PO_4-$(CH_2CH_2O)_6$-ssDNA sequence was purchased from ATDbio (University of Southampton) and prepared as previously described. 1μM ssDNA was co-immobilized with 1mM MCH (10% ethanol) in the molar fraction 1:5 (DNA/total thiol) in 0.8 M phosphate buffer (PB) + 1.0 M NaCl + 5 mM $MgCl_2$ + 1 EDTA, pH 7.0, for 16 h at 4 ^{o}C. The electrode pretreatment and sample preparation was the same described in this chapter and in Section 3.4.3.

After immobilization, electrodes were rinsed with 10mM PB and backfilled with 1 mM MCH (10% ethanol) for 1 h at room temperature. Electrodes were rinsed with water. The electrochemical characterization was performed in 2 mM ferri/ferrocyanide in 50 mM PB + 100 mM K_2SO_4, pH 7.0. Hybridization were

performed using complementary sequencies in the same buffer for 30 min.

The EIS responce, Figure 4.10, demonstrates the R_{ct} increase as a function of target DNA concentration.

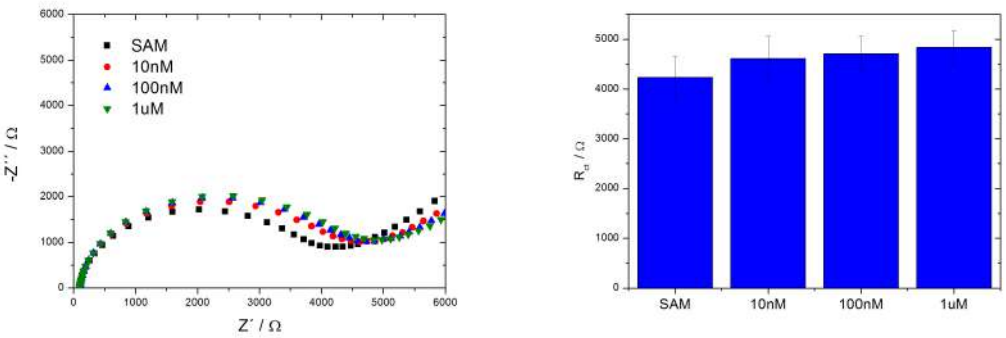

(a) (b)

Figure 4.10: *The HS-$(CH_2)_6$-PO_4-$(CH_2CH_2O)_6$-ssDNA sequence co-immobilized with MCH in 1:5 molar fraction. In (a) the EIS responce to 10nM, 100nM and 1μM target DNA. In (b) the R_{ct} increase for each target DNA concnetration.*

The R_{ct} values from $(CH_2)_6$ linker, previously presented in this chapter, for the SAM are greater than the values from $(CH_2)_6$-PO_4-$(CH_2CH_2O)_6$ shown in this section. The increase in probe length reduces it immobilization on the electrode surface, reducing the charge transfer resistance. However, the linker does not show a relevant influence in the hybridization event.

4.5 BioFET and QCM sensor for DNA hybridization

Label-free detection of DNA hybridization has been achieved by employing different techniques. Electrochemical detection is the main technique due to the intrinsic negative charge from de oligonucleotides and is extremely promising. However, others approches can provide complementary information about the system or reduce the cost, developing reliable sensors with low cost.

QCM can provide valuable and real-time information on the status of the SAM, as the amount of mass absorbed and the viscoelastic properties [8]. In this case, the same platform was tested on QCM to compare the detection.

An other option already reported for DNA hybridization is the Field Effect

Transistor (FET). This class of devices has low cost and can also be easily integrated into portable systems.

4.5.1 Hybrization detection using QCM

QCM measurements were carried out in Q-Sense System (QCM-D, E4) using 5MHz sensor crystals with 14 mm diameter, AT-cut, covered with gold. The crystals were first sonicated in ethanol for 15 min followed by 1 min in piranha solution (1:3 hydrogen peroxide solution and concentrated sulfuric acid). Cleaned crystals were rinsed successively with ultrapure water and dried with nitrogen gas.

The crystals were modified with 300 μl of 1:5 (ssDNA:total thiol) in the I-BFR, for 16h, at 4 ^{o}C. After that, the modified crystals are rinsed with E-BFR and put in the QCM system to stabilize with E-BFR. The oscillator is excited at its fundamental resonance frequency and integer odd multiples and the resonance frequency and energy dissipation changes were monitored. In this case, the fundamental frequency and 3rd, 5th, 7th and 9th overtones are monitored.

After stabilization of the system at 25 ^{o}C, different concentrations of target DNA were injected at 100 μl/min and the flow was turned off. After 30 min E-BFR was injected to remove the remaining tDNA. In Figure 4.12 from 1 fM to 100 pM tDNA were injected over the time. The Δf is show in Table 4.2 with the respective values of Δm and the amount of hybridized molecules.

In an other crystal the same procedure was reproduced injecting higher concentrations of tDNA (Figure 4.12). The 10nM was injected and after washing the Δf correspond to - 200 Hz. When 1 μM was injected the frequenct decreased more 84 Hz.

The Δf was applied in Sauerbrey equation (2.31) to determine Δm value, where, the C_Q was replaced to 17.7 Hz.ng.cm^{-2}, a typical value for 5 MHz crystals and n correspond to 3. The amount of hibridized DNA (Γ) value was calculated considering:

$$\Delta_m = \frac{MW.\Gamma}{N_A} \tag{4.1}$$

The target DNA has molar weight (MW) equal to 6749 g/mol. The result for each concentration is presented in Table 4.2.

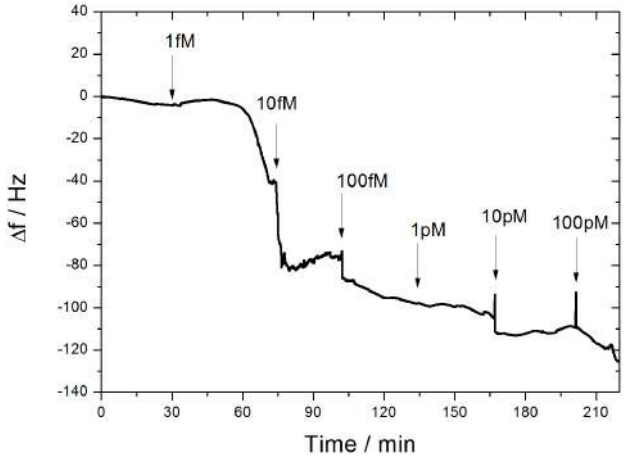

Figure 4.11: *Real-time curve of frequency response for 3th overtone upon small target DNA concentration in flow-condition. Arrows indicate the injection of target DNA over the time.*

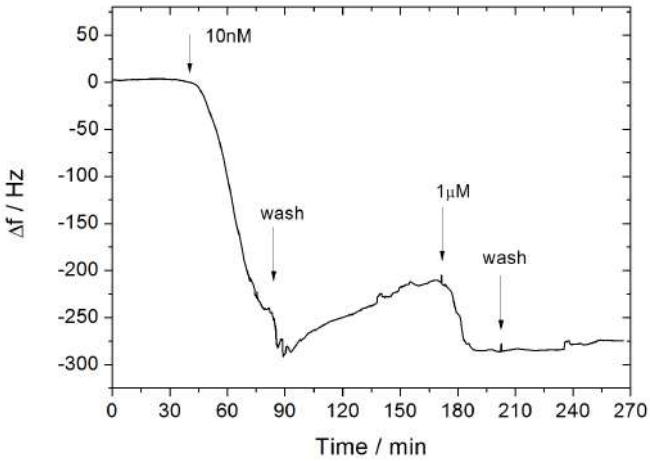

Figure 4.12: *Real-time curve of frequency response for 3th overtone upon increasing target DNA concentration in flow-condition. Arrows indicate the injection of target DNA and E-BFR to wash.*

The information from Table 4.2 can also be interpreted according Figure 4.13, where in (a) the frequency decrease linearly from 1 fM to 100 fM and from 100 pM to 1 μM. This correspond to a similar behavior on mass charge. The range between 100 fM and 10 pM presented a small decrease in frequency that can be related to sample homogeneity.

Table 4.2: *Amount of DNA hibridized. From Figure 4.11 and 4.12 were extracted the Δf, Δm and the theoretical amount of DNA.*

tDNA concentration	Δf (Hz)	Δm (ng)	Γ_0 (10^{13} cm^{-2})
1fM	- 39	230.1	2.0
10fM	- 79	466.1	4.15
100fM	- 97	572.3	5.1
1pM	- 103	607.7	5.4
10pM	- 111	644.9	5.7
100pM	- 119	702.1	6.2
10nM	- 200	1180	10.5
1μM	- 284	1675.6	14.9

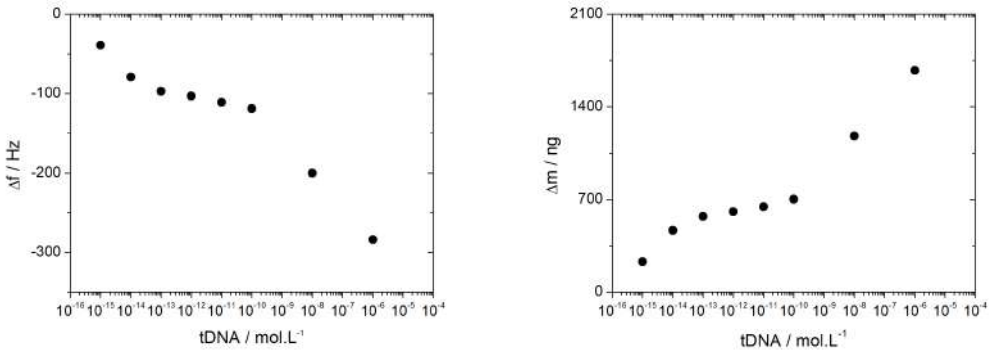

(a) (b)

Figure 4.13: *Information from Table 4.2. The frequency response over the target DNA concentration in (a) and the change of mass over the target DNA concentration in (b).*

Comparing the QCM results with the surface probe density presented in Table 4.1, is possible to verify that QCM show a hibridization 10x higher than the probe density. The QCM electrode has a roughness greater than the others electrodes, which increase the surface area or the real area. The probe surface density was calculated using Cottrell equation and considering the real area from the potenciostat electrodes. Now, this approach can not be compare with QCM system. Even though, QCM show a interesting correlation.

4.5.2 BioFET detection

The detection is based on the modulation of the gate voltage associated with the increased negative charge on the gate upon hybridization. The method can be applied to other bio-reactions that result in a modification of surface charge.

Using an instrumental amplifier the potentiostat electrode was connected to the gate of the EGFET system after the surface modification with SAM (1:4). Each potential value was redorded over 5 minutes for five different samples in E-BFR without redox marker.

The electrodes were incubated with different target sequence concentration for 30 min. After the incubation, the electrodes were rinsed with E-BFR and connected to the gate. The potential average over the 5 minutes was calculated and presented in Figure 4.14.

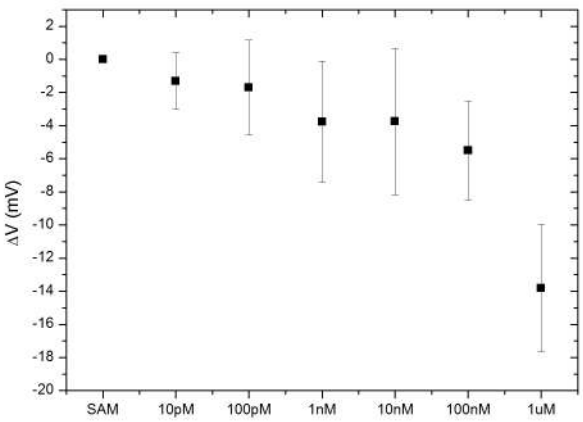

Figure 4.14: *Difference of potential as a function of the target DNA concentration. Hybridization is performed at E-BFR without redox marker in solution.*

The increase of negative charge in the gate due to hybridization leads to a shift in the potential. However, the results presented a high standard deviation between the samples, with low reproducibility and low detection.

The FETs are a class of low-cost device that can be improved through signal amplification and explored in futures works for biomarkers recognition.

Chapter 5

HER2 aptamer

Breast cancer is one of the most common cancers and the second cause of women deaths [41, 42]. More than 90% of these deaths are related to metastatic growth [41]. Therefore, early stage detection of cancer is crucial to increase the chances of survive. Human epidermal growth factor receptors (HER/erbB) are involved in normal growth and cell differentiation. A malignant growth can be related with HER2 overexpression and it is present in some cases of breast, ovarian, lung, gastric, oral, prostate and other cancers [43].

HER2 has been shown overexpressed in around 20-30% of aggressive breast cancers and associated with poor-prognosis [42]. Breast cancer patients have high HER2 concentrations in their blood (15-75 ng/mL) compared to normal individuals (2-15 ng/mL) [44, 45]. To evaluate these concentrations, different HER2 detection techniques have been reported, including fluorescence in situ hybridization (FISH) assays and immunohistochemical (IHC) assays [46]. However, these techniques require sophisticated instrumentations, special training, are labour-intensive and time-consuming.

To satisfy these unmet clinical needs, several biosensors that recognize enzymes, receptors and antibodies have been reported [47, 48]. One of the disadvantages of using antibodies is their instability due to irreversible denaturation. Therefore, alternative biorecognition elements are demanding to develop stable biosensors. Synthetic molecules such as aptamers can fulfil these gaps associated with biomarkers. Aptamers are single strand oligonucleotides (DNA or RNA) that are design to bind specific targets, as proteins [49]. The unique aptamers property has shown great potential for biosensors using optical, electrochemical,

and mass-sensitive approaches [49, 50].

In the recent years, several electrochemical aptasensors based on Faradaic approach have been reported for the detection of cancer specific antigens, but just few of them are focused on HER2. In this study, gold electrodes were modified with DNA aptamers [51] designed to specifically bind HER2 protein. The electrochemical impedance spectroscopy was used to characterize binding events.

5.1 Biosensor Fabrication

5.1.1 Materials

All DNA aptamer sequences were purchase from Sigma-Aldrich. Recombinant human ErbB2 / HER2 Fc Chimera protein were purchased from R&D Systens (Bio-Techne, Minneapolis, MN, USA). All chemical used in the experiments were also purchased from Sigma-Aldrich and used as received. The aqueous solutions were prepared using Ultra-pure water (Millipore) with a Biopak Polisher Ultrafilter (CDUFBI001) filter to remove pyrogen, nuclease and protease and filter with 0.22 μm syringe filter before use.

5.1.2 Sample preparation

Thiol-modified probe were prepared adding a specific volume of TE buffer to obtain 100 μM. HER2 protein are prepared adding a specific volume of phosphate buffered saline (0.01 M phosphate buffer, 0.0027 M potassium chloride and 0.137 M sodium chloride, pH 7.4) to obtain 100 μM. Both samples are divided in small aliquots and frozen at - 20 ^{o}C until use. The aptamer sequence tested are shown in Table 5.1.

Table 5.1: *DNA aptamer sequences. The two sequences tested for aptasensor development.*

Probe	5' -HS$(CH_2)_6$ - Sequence - 3'
1	AACCGCCCAAATCCCTAAGAGTCTGCACTTGTCATTTTGTATA TGTATTTGGTTTTTGGCTCTCACAGACACACTACACACGCACA
2	ATTAAGAACCATCACTCTTCCAAATGGATATACGACTGGG

5.1.3 Electrode preparation

HER2 aptamers were heated to 95°C for 10 min and cooled immediately on ice for 15 min. MCH is first diluted in ethanol (BioUltra) (100 mM) and then, rediluted in water (10%) to obtain 1 mM. DNA aptamer immobilization buffer (I-BFR) consisted of 0.8 M phosphate buffer (PB) + 1.0 M NaCl + 5 mM $MgCl_2$ + 1 EDTA, pH 7.0. Aptamer and MCH are co-immobilized on the top of clean electrodes (according to section 3.2.1) for 16 h at 4 ^{o}C.

After immobilization, the same procedure for DNA in the last chapter is repeated. Electrodes were sequentially rinsed in I-BFR followed by 200mM PB, 10mM PB + 10mM EDTA and finally 10mM PB to remove any remaining Mg^{2+}. To ensure the complete thiol coverage of the gold surface, the electrodes were backfilled with 1 mM MCH (10%) immersion for 1 h at room temperature. Electrodes were finally rinsed with water.

The aptasensor is exposed to differrent concentrations of HER2 protein in PBS for 30 min. All the electrochemical characterization was performed in 2.5 mM ferro/ferricyanide in PBS.

For surface plasmon resonance (SPR) experiments, gold coated SPR sensors were immobilized with the aptamer overnight and measurements carried out in 10 mM PBS under flow conditions. The flow rate was kept constant at 25 l/min upon injection of 50nM HER2 and ACT-PSA protein for 10 min binding and followed by 5 min for dissociation of unbound protein.

5.1.4 Instrumentation

All electrochemical characterizations were carried out in an electrochemical cell with the 3 electrodes configuration, using a $Hg/HgSO_4$ electrode (FATEC) as the reference electrode and a platinum wire as the counter electrode (Metrohm). An Autolab PGSTAT20 (Metrohm) was used to perform the electrochemical experiments with a FRA module. SPR experiments were carried out in a dual-channel SPR7000DC from Reichert Technologies (Depew,NY, USA).

5.2 Electrochemical characterization of modified electrodes

The aptasensor development started in the University of Bath (UK) using probe 1 [51]. The method applied for aptasensor is similar to the previous one for DNA hybridization sensor. DNA aptamers has also negative charge and interact with the redox probe (ferri/ferro) in solution repelling it.

The first sequence was one of the few HER2 aptamers in the literature until 2015. The predicted second structure is illustrated in Figure 5.1.

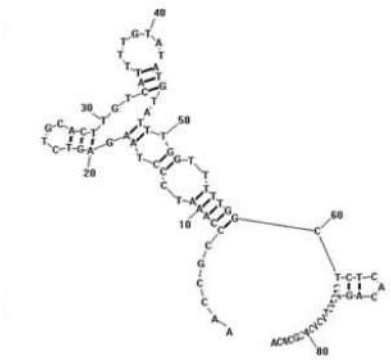

Figure 5.1: *Predicted aptamer 1 secondary structures. Reproduced from [51].*

Most of the aptasensors already developed use DNA sequences between 20 - 40 nucleotides, however, this sequence has more than 80 nucleotides. The increase in the probe lengh leads to increase in the size of the secondary structure, which, in electrode surface, cover a large area. Therefore, the molar fraction between the aptamer and the MCH tested was 1:100, 1:200 and 1:500. Figure 5.2 presents the the percentage of R_{ct} increase after 1μM HER2 binding for 30min.

The maximum percentage change of charge transfer resistance upon binding was obtained from DNA aptamer probe electrodes co-immobilized with MCH at a molar fraction of 0.5%, where the R_{ct} increased 35.61% compared to 10.05% and 19.9% for 1:100 and 1:500 respectively. Negative controls were conducted using HER4 proteins. The few electrodes tested were not sufficient to ensure reliable statistical values, but indicate that the aptamer has low non-specific binding.

The electrodes modified with aptamers are also negatively charged as the DNA sequences presented in the previously chapters. The protein binding leads to

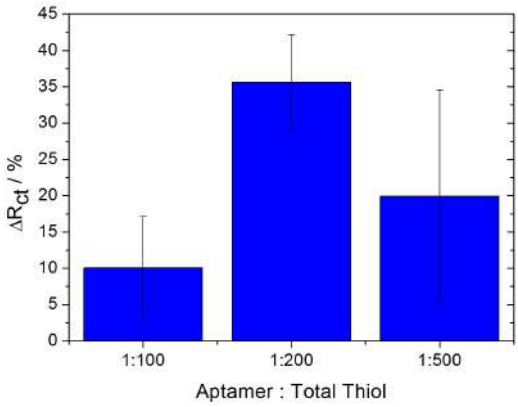

Figure 5.2: *Influence of different molar fraction in R_{ct}. Electrodes were co-immobilized with HER2 aptamer and MCH in different molar fraction. The bars show the R_{ct} after 1μM HER2 binding for 30min.*

an increase of charge transfer resistance due to a high mass loading on the surface of the electrodes, which will reduce the redox probe approaching the surface. However, when the system was tested with low HER2 protein concentration, close to human values, the aptasensor presented a non-linear behavior with insignificant R_{ct} increase.

An other point that has to be considered is the Kd value or dissipation constant. The smaller the Kd value, the greater is the binding affinity of the aptame for its target. In this case Kd = 18.9nM, which correspond to a low value as necessary.

Surface plasmon resonance was used to test the aptasensor with low HER2 concentrations. Figure 5.3 shows the results for 50nM HER2 and the same concentration of non-specific ACT-PSA protein. After removing the unbound protein, the specific binding is 72.7% higher than the non-specific.

SPR as an optical technique is able to detect the binding event in lower concentrations than EIS. In this specific system, the huge sequence length can lead to binding events far from the electrode surface and, consequentetly, out of the double layer. In this case, the electrochemical techniques are not able to detect.

In 2016 new HER2 aptamers were reported using a small DNA sequence, described in Table 6.1 as probe 2. This sequence is illutrated in Figure 5.4.

The second aptamer tested has 40 nucleotides and Kd = 28.6nM [52]. Comparing to the DNA sequences from chapter 3, 4 and 5 is the double, but at the

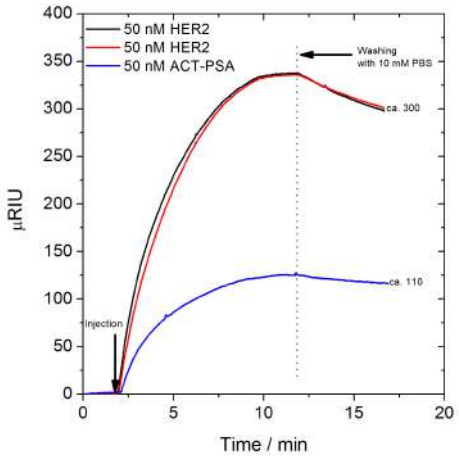

Figure 5.3: *SPR specific and non-specific binding. The aptamer was tested with 50nM of HER2 and AT-PSA.*

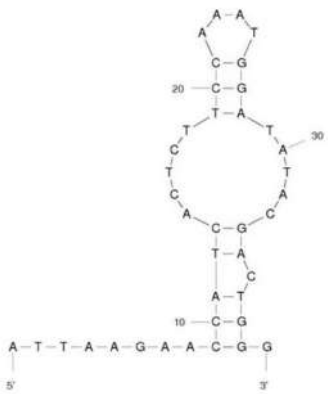

Figure 5.4: *Predicted aptamer secondary structures for probe 2. Reproduced from [52].*

same time, half of the first one. The predicted secondary structure is directly related with the sequence length and, consequentetly, with the aptamer molar fraction on the electrode surface.

Co-immobilized aptamer with MCH was tested with 1:5, 1:10, 1:50 and 1:100 molar fractions. The charge tranfer resistance results for binding with 1μM HER2 are presented in Figure 5.5(a). The increase corresponds to 3.5, 4.1, 9.3 and 6.4% respectively.

The maximum percentage R_{ct} upon binding was obtained from DNA aptamer probe electrodes co-immobilized with MCH at a molar fraction of 2.0%. Electrodes

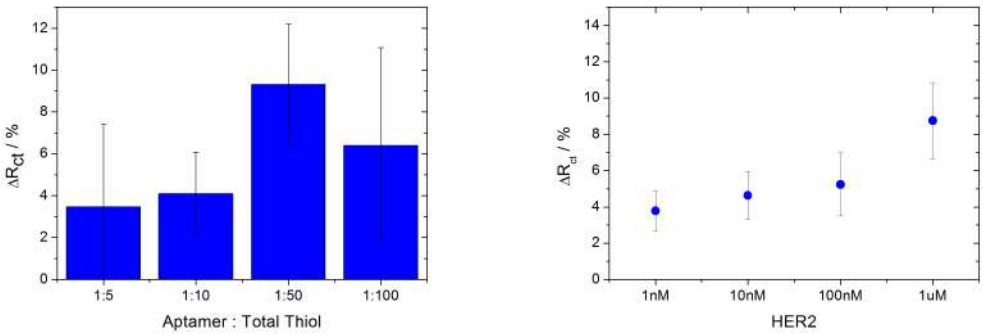

(a) (b)

Figure 5.5: *Aptasensor detection. Co-immobilized aptamer with MCH was tested with 1:5, 1:10, 1:50 and 1:100 molar fractions with 1μM of HER2 protein (a). The optimized molar fraction (1:50) was tested with different HER2 concentrations using EIS (b).*

with this molar fraction were exponsed sequentially from 1 nM to 1 μM of HER2 protein concentration. The R_{ct} responce is show in Figure 5.5(b). The human values of interest come from 1 nM to 10 nM. For this range the aptasensor respond to the presence of specific protein. However, it was not possible to obtain an analytical curve.

The aptasensors for HER2 protein presented promising results. However, further improvements are required to conclude the linear range for detection and its limit with the necessary reliability.

Chapter 6

Conclusion

Label-free DNA biosensor was investigated to detect target analyte in solution using different techniques. Electrochemical transduction was explored through cyclic voltammetry, electrochemical impedance spectroscopy and chronocoulometry, followed by quartz crystal microbalance and biofet where the same parameters were reproduced. The oligo sequence used as probe and target correspond to a DNA form of microRNA 200a, related with breast and ovary cancer.

The platform was first optimized starting with the immobilization procedure, including electrode cleaning, probe and spacer immobilization, buffers and probe density quantification. The electrode surface roughness or the real area was determined by electrochemical cleanning and limited to 1.5 x geometric area. High ionic strenght immobilization buffer combined with co-immobilization of probe and spacer gives a better quality in terms of probe orientation, control of probe density and reproducibility. This procedure follow by backfilling with high concentration of spacer avoid non-specific interation.

Immobilization procedure was optimized using cyclic voltammetry and electrochemical impedance spectroscopy. The probe surface density was determined through chronocoulometry. For that, a mix using different molar fraction of probe and spacer were prepared in the immobilization buffer. This method provide an effective control of probe surface density. A linear relationship between molar fraction and probe surface density was observed changing the probe from 10 to 50% and getting as result from 2.84 to 4.31 x 10^{12} molecules/cm^2.

The optimized system was tested with 1 μM target sequence and the increase of R_{ct} was compared to probe density to obtain the optimized hybridization

efficiency. In this case, 20% of probes on the immobilization buffer leads to the highest increase of the R_{ct} due to hybridization. From these parameters was possible to set up a calibration curve, where 100 fM as limit of detection was observed. This limit is high compared with the literature, however any amplification was used and the platform was able to distinguish non-specific sequences with 4 mismatch bases decreasing more than 80% of the R_{ct}.

The platform was reproduced on top of QCM electrodes considering the same parameters. The frequency decrease with the hibridization over different target concentrations. The frequency can be used to estimate the density of target sequences that hybridized. However, the values are higher that the probe surface density estimated electrochemically. In this case, the real area of QCM electrodes are higher due to it roughness, which also affects the area value used on Cottrell equation.

The bulk gold electrode modified with SAM was also connected with the gate of the EGFET system using an instrumental amplifier. The charge increased on the electrode surface due to hybridization was just able to detect high concentrations of target DNA. This low cost detection have to be improved with further signal amplification.

For the system used in this work, further improvement on performance are required, such as nanoparticles or DNA intercalators for signal amplification. The electrode modification presented here has a classical approach, however, different different surface modifications already reported show it as a possibility.

Aptamers are single strand of DNA or RNA that as design to bind proteins with high affinity and specificity. The same SAM was developed replacing the short ssDNA by DNA aptamer with a longer sequence. In this case, two different HER2 aptamers bind the target with different dissociation coeffcient and have different sequence length. The effect of these parameters are reflected on the bind event identification. The increase of sequence length increase the binding event from the SAM surface, decreasing the detection. At the same time, low dissociation coeffcient are required to increase the detection. Playing with these parameters were possible to optimized the platform for HER2 detection. However, further improvements are required to distinguish low variations on clinically relevant values.

Promising results have been achieved from the study of DNA hybridization sensor system. The electrochemical impedance spectroscopy proved to be a versatile technique for biomarker detection supported by other electrochemical techniques. The biosensor platform can also be reproduced using other transducing or even others biomarkers. This first study opened the way for a lot of possibilities of biomarker detection and improvements.

References[1]

[1] WATSON, J. D.; CRICK, F. H. C. Molecular structure of nucleic acids. *Nature*, p. 737–738, 1953.

[2] ELEY, D.; SPIVEY., D. I. Semiconductivity of organic substances. part 9. nucleic acid in the dry state. *Trans. Farday Soc.*, v. 58, p. 411, 1962.

[3] DRUMMOND, T. G.; HILL, M. G.; BARTON, J. K. Electrochemical dna sensors. *Nature Biotechnology*, v. 21, p. 1192 – 1199, 2003.

[4] THEVENOT, D. R. et al. Electrochemical biosensors: recommended definitions and classification. *Biosensors & Bielectronics*, v. 16, p. 121–131, 2001.

[5] KEIGHLEY, S. D. et al. Optimization of dna immobilization on gold electrodes for label-free detection by electrochemical impedance spectroscopy. *Biosensors and Bioelectronics*, v. 23, p. 1291–1297, 2008.

[6] JOLLY, P. et al. Highly sensitive dual mode electrochemical platform for microrna detection. *Scientific Reports*, v. 6, p. 36719, 2016.

[7] GOPINATH, S. C. et al. Aptamer-based 'point-of-care testing. *Biotechnology Advances*, v. 34, p. 198–208, 2016.

[8] FORMISANO, N. et al. Optimisation of an electrochemical impedance spectroscopyaptasensor by exploiting quartz crystal microbalance with dissipationsignals. *Sensors and Actuators B*, v. 220, p. 369–375, 2015.

[9] DENNISON, M. J.; TURNER, A. P. F. Biosensors for environmental monitoring. *Biotechnology Advances*, p. 1–12, 1995.

[1] According to Brazilian Association of Technical Standards (ABNT). NBR 6023.

[10] PRODROMIDIS, M. I.; KARAYANNIS., M. I. Enzyme based amperometric biosensors for food analysis. *Electroanalysis*, p. 241–261, 2002.

[11] TSIAFOULIS, C. G.; PRODROMIDIS, M. I.; KARAYANNIS, M. I. Development of amperometric biosensors for the determination of glycolic acid in real samples. *Analytical Chemistry*, p. 132–139, 2002.

[12] BARD, A. J.; FAULKNER, L. R. *Electrochemical Methods: Fundamentals and Applications*. 2nd. ed. [S.l.]: Wiley, 2000. ISBN 978-0-471-04372-0.

[13] WANG, H.; PILON, L. Accurate simulations of electric double layer capacitance of ultramicroelectrodes. *J. Phys. Chem. C*, v. 115, p. 16711–16719, 2011.

[14] STOJEK, Z. *Electroanalytical Methods*. 2nd. ed. [S.l.]: Springer, 2009. ISBN 978-3-642-02914-1.

[15] BRADSHAW, L. Understanding piezoelectric quartz crystals. *RF time and frequency*, v. 8, p. 50–58, 2000.

[16] RODAHL, M. et al. Simultaneous frequency and dissipation factor qcm measurements of biomolecular adsorption and cell adhesion. *Faraday Discuss*, v. 107, p. 229–246, 1997.

[17] SAUERBREY, G. Verwendung von schwingquarzen zur wagung dunner schichten und zur mikrowagung. *Zeitschrift fur Physik*, v. 155, p. 206–222, 1959.

[18] NOMURA, T.; MINEMURA, A. Behavior of a piezoelectric quartz crystal in an aqueous solution and the application to the determination of minute amount of cyanide. *Chemical Society of Japan*, v. 10, p. 1621–1625, 1980.

[19] BARD, A. J.; FAULKNER, L. R. *Electrochemical DNA Biosensors*. 1st. ed. [S.l.]: Pan Stanford Publishing Pte. Ltd., 2012. ISBN 978-981-4303-98-9.

[20] BERGVELD, P. Development of an ion-sensitive solid-state device for neurophysiological measurements. *Ieee Trans, Biomed. Eng.*, v. 70, p. BM17, 1970.

[21] SPIEGEL, J. van der et al. Teh extended gate chemically sensitive field effect transistor as multi-species microprobe. *Sens. Actuators*, v. 4, p. 291–298, 1983.

[22] LOVE, J. C. et al. Self-assembled monolayers of thiolates on metals as a form of nanotechnology. *Chemical Reviews*, v. 4, p. 1103–1169, 2005.

[23] CARVALHAL, R. F.; FREIRE, R. S.; KUBOTA, L. T. Polycrystalline gold electrodes: A comparative study of pretreatment procedures used for cleaning and thiol self-assembly monolayer formation. *Electroanalysis*, v. 17, p. 1251–1259, 2005.

[24] TOMBELLI, S.; MASCINI, M.; TURNER, A. P. F. Improved procedures for immobilisation of oligonucleotides on gold-coated piezoelectric quartz crystals. *Biosensors & Bioelectronics*, v. 17, p. 929–936, 2002.

[25] STEEL, A. B.; HERNE, T. M.; TARLOV, M. J. Electrostatic interactions of redox cations with surface-immobilized and solution dna. *Bioconjugate Chemistry*, v. 10, p. 419–423, 1999.

[26] STEEL, A. B. et al. Immobilization of nucleic acids at solid surfaces: Effect of oligonucleotide length on layer assembly. *Biophysical Journal*, v. 79, p. 975–981, 2000.

[27] HOOGVLIET, J. C. et al. Electrochemical pre-treatment of polycrystalline gold electrodes to produce a reproducible surface roughness for self assembly: A study in phosphate buffer ph 7.4. *Analytical Chemistry*, v. 72, p. 2016–2021, 2000.

[28] RON, H.; MATLIS, S.; RUBINSTEIN, I. Self-assembled monolayers on oxidized metals. 2. gold surface oxidative pretreatment, monolayer properties, and depression formation. *Langmuir*, v. 15, p. 1116–1121, 1998.

[29] RON, H. H.; RUBINSTEIN, I. Alkanethiol monolayers on preoxidized gold-encapsulation of gold oxide under an organic monolayer. *Langmuir*, v. 10, p. 4566–4573, 1994.

[30] LAO, R. J. et al. Electrochemical interrogation of dna monolayers on gold surfaces. *Analytical Chemistry*, v. 77, p. 6475–6480, 2005.

[31] KHOSRAVINIA, H.; RAMESHA, K. P. Influenca of edta and magnesium on dna extraction from blood samples and specificity of polymerase chain reaction. *African Journal of Biotechnology*, v. 6, p. 184–187, 2007.

[32] STEEL, A. B.; HERNE, T. M.; TARLOV, M. J. Electrochemical quantitation of dna immobilized on gold. *Analytical Chemistry*, v. 70, p. 4670–4677, 1998.

[33] ESTRELA, P. et al. Label-free sub-picomolar protein detection with field-effect transistors. *Anal. Chem.*, v. 82, p. 3531–3536, 2010.

[34] LUCARELLI, F. et al. Electrochemical and piezoelectric dna biosensors for hybridization detection. *Anal. Chem.*, v. 602, p. 139–159, 2008.

[35] HU, P. et al. Self-assembled nanotube field-effect transistors for label-free protein biosensors. *Journal of Applied Physics*, v. 104, p. 074310, 2008.

[36] HENEGHAN, H. M.; MILLER, N.; KERIN, M. J. Mirnas as biomarkers and therapeutic targets in cancer. *Current Opinion in Pharmacology*, v. 10, p. 543–550, 2010.

[37] LEE, R.; FEINBAUM, R. L.; AMBROS, V. The c. elegans heterochronic gene lin-4 encodes small rnas with antisense complementarity to lin-14. *Cell.*, v. 75, p. 843–54, 1993.

[38] ZHANG, B. et al. microrna as oncogenes and tumor suppressors. *Developmental Biology*, v. 302, p. 1–12, 2007.

[39] ESTRELA, P. *Essays in Biochemistry*. 1st. ed. [S.l.]: Portland Press, 2016. ISBN 978-1-85578-199-3.

[40] HUMPHRIES, B.; YANG, C. The microrna-200 family: small molecules with novel roles in cancer development, progression and terapy. *Oncotarget*, v. 6, p. 6472–98, 2015.

[41] SIEGEL, R.; NAISHADHAM D., J. A. D. Cancer statistics,2013. *CA Cancer J. Clin.*, v. 63, p. 11–30, 2013.

[42] DIACONU, I. et al. Electrochemical immunosensors in breast and ovarian cancer. *Clin. Chim. Acta*, v. 425, p. 128–138, 2013.

[43] PATRIS, S. et al. Nanoimmunoassay onto a screen printed electrode for her2 breast cancer biomarker determination. *Talanta*, v. 130, p. 164–170, 2014.

[44] HUNG, M. et al. Her-2 neu-targeting gene therapy - a review. *Gene*, v. 159, p. 65–71, 1995.

[45] CHUN, L. et al. Electrochemical detection of her2 using single stranded dna aptamer modified goldnanoparticles electrode. *Sens. Actuat. B: Chem.*, v. 186, p. 446–450, 2013.

[46] PRESS, M. et al. Evaluation ofher-2/neu gene amplification and overexpression: comparison of frequently used assay methods in a molecularly characterized cohort of breast cancer specimens. *J. Clin. Oncol.*, v. 20, p. 3095–3105, 2002.

[47] CAMACHO, C. et al. Novelenzyme biosensor for hydrogen peroxide via supramolecular associations. *Biosens. Bioelectron.*, v. 24, p. 2028–2033, 2009.

[48] NOLTE, D. Prostate-specific antigen immunoassays on the biocd. *Anal. Bioanal. Chem.*, v. 393, p. 1151–1156, 2009.

[49] QURESHIA, A.; GURBUZB, Y.; NIAZIA, J. Label-free capacitance based aptasensor platform for the detection ofher2/erbb2 cancer biomarker in serum. *Sensors and Actuators B*, v. 220, p. 1145–1151, 2015.

[50] CHO, E.; LEE, J.; ELLINGTON, A. Applications of aptamers as sensors. *Ann. Rev.Anal. Chem.*, v. 2, p. 241–264, 2009.

[51] LIU, Z. et al. Novel her2 aptamer selectively delivers cytotoxic drug to her2-positive breast cancer cells in vitro. *Journal of Translational Medicine*, v. 10, p. 148, 2012.

[52] GIJS, M. et al. Improved aptamers for the diagnosis and potential treatment of her2-positive cancer. *Pharmaceuticals*, v. 9, p. 29, 2016.

[53] HOLLIDAY, D.; SPEIRS, V. Choosing the right cell line for breast cancer research. *Holliday and Speirs Breast Cancer Research*, v. 13, p. 215, 2011.

[54] ALTOGEN. *MCF-7 Cells human breast adenocarcinoma cell line*. 2016. `http://www.mcf7.com`. [Online; accessed 15-Jun-2016].

[55] BARTEL, D. P. Microrna: genomics, biogenesis, mechanism, and function. *Cell*, v. 116, p. 281–97, 2004.

[56] LAWRIE, S. G. C. H.; DUNLOP, H. M. Detection of elevated levels of tumour-associated microrna in serum of patients with diffuse large b-cell lymphoma. *Br J Haematol*, v. 141, p. 672–5, 2008.

[57] CUK, K. et al. Circulating microrna in plasma as early detection markers for breast cancer. *Int. J. Cancer*, v. 132, p. 1602–1612, 2013.

[58] JURMEISTER, S. et al. Microrna-200c represses migration and invasion of breast cancer cells by targeting actin-regulatory proteins fhod1 and ppm1f. *Molecular and Cellular Biology*, v. 32, p. 633–651, 2012.

[59] BANDO MASAKAZU TOI, K. K. H.; KOIKE, M. Genes commonly upregulated by hypoxia in human breast cancer cells mcf-7 and mda-mb-231. *Biomedicine & Pharmacotherapy*, v. 57, p. 333–340, 2013.

[60] HAMDAN, F. H.; ZIHLIF, M. A. Gene expression alterations in chronic hypoxic mcf7 breast cancer cell line. *Genomics*, v. 104, p. 477–481, 2004.

[61] WESTERMEIER, R. Gel electrophoresis. *ENCYCLOPEDIA OF LIFE SCIENCES*, p. 1–6, 2005.

[62] COMPANY, T. B. E. *Principles and Practice of Agarose Gel Electrophoresis*. 2016. `https://www.wou.edu/las/physci/ch462/Gel%20Electrophoresis.pdf`. [Online; accessed 15-Jun-2016].

[63] EUROGENTEC. *qPCR Guide*. 2016. `http://www.eurogentec.com/uploads/qPCR-guide.pdf`. [Online; accessed 15-Jun-2016].

[64] RAD, B. *What is Real-Time PCR (qPCR)?* 2016. `http://www.bio-rad.com/pt-br/applications-technologies/what-real-time-pcr-qpcr`. [Online; accessed 15-Jun-2016].

[65] MAHMOOD, T.; YANG, P.-C. Western blot: Technique, theory, and trouble shooting. *North American Journal of Medical Sciences*, v. 4, p. 429–34, 2012.

[66] SHEN, G. et al. Hypoxia-regulated micrornas in human cancer. *Acta Pharmacol Sin*, v. 34, p. 336–341, 2013.

Appendix A

Biological Aspects

Cell lines are widely used in laboratory and particularly as in vitro models in cancer research. They have a number of advantages as, easy to handle and represent an unlimited selfreplicating source that can be grown in almost infinite quantities, a relatively high degree of homogeneity and are easily replaced from frozen stocks if lost through contamination [53].

The first breast cancer cell line was established in 1958. 20 years later breast cancer cell lines became more widespread. The most commonly used breast cancer cell line in the world, MCF-7 was established in 1973 at the Michigan Cancer Foundation [53].

MCF-7 was first isolated in 1970 from the breast tissue of a 69 year old Caucasian woman. Since then this cell line has been widely studied [54]. The popularity of MCF-7 is largely due to its exquisite hormone sensitivity through expression of estrogen receptor (ER), making it an ideal model to study hormone response. Relatively few breast cancer cell lines have been established in the more recent past [53]. Therefore, this was the cell line chosen fot this study.

MiRNAs were described on chapter 4 as a small (18-25 nucleotides), noncoding RNAs that regulate gene expression on a post-transcriptionallevel by degrading mRNA molecules or blocking their translation [55]. Hence, they play an essential role in the regulation of a large number of biological processes, including cancer.

Lawrie et al. were the first to demonstrate the presence of circulating miRNAs in cell-free bodily fluids such as plasma and serum [56]. Since then, circulating miRNAs have been reported as being expressed in blood plasma or serum

in different types of cancer, e.g., prostate, colorectal and esophageal carcinoma[57].

Expression of miR-200 family members is frequently down-regulated in metastases compared to that in primary tumors, and reduced miR-200 levels are associated with a poor outcome in several human epithelial malignancies . Furthermore, overexpression of miR-200 was demonstrated to suppress metastasis in mouse models of lung adenocarcinoma and breast cancer [58].

The PhD project in Brazil and at University of Bath developed a biosensor with singles strands of miRNA-200a synthetic sequence immobilized. Therefore, this part of the project focus on show some biological aspects of miRNA extraction from breast cancer cell line in two different situations, normoxia and hypoxia.

Most solid tumors contain hypoxic parts. Hypoxia affects a variety of tumor-associated events as cell growth rate, metastasis and sensitivity to treatment [59]. Recent reports revealed that the status of hypoxia in tumor tissue is a marker of poor prognosis in several types of solid cancers including carcinoma of the uterine cervix, head and neck cancers, brain tumors and breast cancer. Around 40% of all breast cancer and half of the locally advanced breast cancers include regions affected by hypoxia [60].

It is postulated that hypoxia-induced differentiation is a mechanism of tumor progression. From the therapeutic point of view, a number of data demonstrated that oxygen concentration alters the sensitivity of chemotherapeutic agents [59].

Therefore, it would be beneficial to characterize and identify genes up and downregulated by hypoxia in cancer. Many studies have already focused upon hypoxia-induced alterations in gene expression. However, specific genetic changes involved in the adaptation of tumors to hypoxia have not yet been fully understood. Therefore, identifying the modulated genes by hypoxia in cancer is great benefit [60].

Techniques

Alterations on cells can be identify using differents techniques. Some of them are used to identify and quantify levels of miRNA expression and other to quantify proteins. Looking for a better understanding different techniques were applied to analize the samples.

Eletrophoresis

Electrophoresis is the migration of charged particles or molecules in an electric field [61]. Agarose gel electrophoresis is a used procedure in various areas of biotechnology. This simple, but precise analytical procedure is used in research, biomedical and forensic laboratories [62]. It is a powerful separation method frequently used to analyze DNA fragments generated by restriction enzymes, and it is a convenient analytical method for determining the size of DNA molecules in the range of 500 to 30,000 base pairs. It can also be used to separate other charged biomolecules such as dyes, RNA and proteins [61].

The horizontal electrophoresis apparatus (Figure 1) is essentially a rectangular box with electrodes at each end. The separation medium is a gel made of agarose, which is a polysaccharide derivative of agar and contains buffer for conductivity.

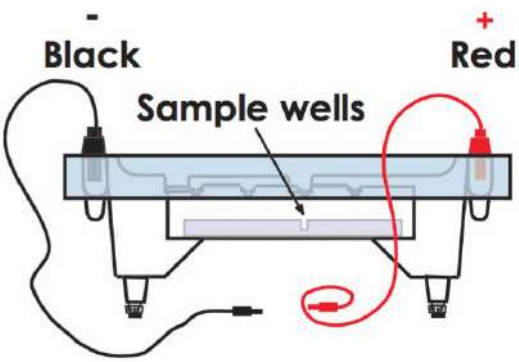

Figure A.1: *Horizontal gel electrophoresis apparatus with the sample inside. Reproduced from [61]*

A power source is connected to the apparatus and a potencial is applied. Charged molecules in the sample enter the gel through the walls of the wells. Molecules having a net negative charge migrate towards the positive electrode. The buffer serves as a conductor of electricity and to control the pH, which is important to the charge and stability of biological molecules [62].

DNA/RNA has a strong negative charge at neutral pH, it migrates through the gel towards the positive electrode during electrophoresis. Gels separating DNA require staining in order to be visualized. Although DNA samples that are prepared for electrophoresis typically appear bluish-purple, the DNA itself does not have color. The color comes from a dye in a gel loading solution that is added at the end

of typical DNA reactions. The gel loading solution stops the reaction [61].

The most commonly used stains for visualizing DNA contain ethidium bromide. Visualization also requires a short wave ultraviolet light source.

The separation occurs because smaller molecules pass through the pores of the gel more easily than larger ones. If the size of two fragments are similar, they will migrate together in the gel. If chromosomal DNA/RNA is cleaved many times, the wide range of fragments produced will appear as a smear after electrophoresis[61].

qPCR

The Polymerase Chain Reaction (PCR) has been invented in 1983 by Kary Mullis (Nobel Price in 1993). Three years after, there was an incredible expansion of its use thanks to the commercialization of the Taq polymerase, a polymerase that resists high temperatures. In 1992, the technique was again improved by the use of Ethidium Bromide, thanks to the fluorescence that results from the binding to duplex DNA. The kinetics of fluorescence accumulation during thermocycling was directly related to the starting number of DNA copies. This was the starting point of Real-Time qPCR [63].

Both PCR and qPCR are widely used technologies today. The principle, and aim, of the PCR technology is to specifically increase a target from an undetectable amount of starting material. In classical PCR, at the end of the amplification, the product can be run on a gel for detection of this specific product. In Real-Time PCR (qPCR), this step can be avoided since the technology combines the DNA amplification with the immediate detection of the products in a single tube.

Current detection methods are based on changes in fluorescence, which are proportional to the increase of target. Fluorescence is monitored during each qPCR cycle providing an amplification plot, allowing the user to follow the reaction in real time.

The steps that need to follow after extract the samples will be:

1. Perform the Reverse Transcription (RT) step before your qPCR assay. The RT step lasts 30 minutes around 50°C. The cDNA generated should be stored at -80°C.

2. Use specific primers, which bind to the gene of interest. In this case,

miRNA-200a primer. The specific primers are used in the PCR step, leading to specific cDNA.

3. Analysis takes the Ct (cycle number) value, at the point when the signal is detected above the background and the amplification is in exponential phase. The more abundant the template sample, the quicker this point is reached, thus giving earlier Ct values. Differences in Ct then have to be correlated to some other quantitative values to make them meaningful.

Double-Dye Oligonucleotides, or Double-Dye Probes are the most widely used type of probes, which consisted of a single-strand probe sequence that was complementary to one of the strands of the amplicon. The Exiqon ® kit comes with LNA (Locked Nucleic Acid). LNA is a bicyclic RNA analogue, in which the ribose moiety in the sugar-phosphate backbone is structurally constrained by a methylene bridge between the 2'-oxygen and the 4'-carbon atoms.

LNA changes the conformation of the helix and increases the stability of the duplex. Increasing the stability of the duplex allows an increase of the melting temperature of the duplex. It is therefore possible to reduce the size of the probe, which increases the specificity of the probe.

Each qPCR cycle is control by a thermocycle increasing and decreasing the temperature according the protocol. One exemple in Figure 1.2 illustrate.

The first step at 50^oC cleaves any contaminating template containing U bases. The 10 minutes step at 95^oC activates the LNA. 15 seconds at 95^oC is the first step of the repeated PCR cycles.

The dsDNA template denatures at this temperature. 60^oC for 1 minute, allows the annealing and extension of the primers by the LNA. Depending on your thermocycler, and the characteristics of your primers, the protocol can be shortened and the temperatures adapted.

To understand the results graphs it is necessary to be familiar with some definitions and concepts. The amplification Curve is usually as Figure 1.3, It shows the increase of fluorescence level on the Y axis, compared to the run cycle number on the X axis.

- The baseline is the average background. It is calculated according to the noise

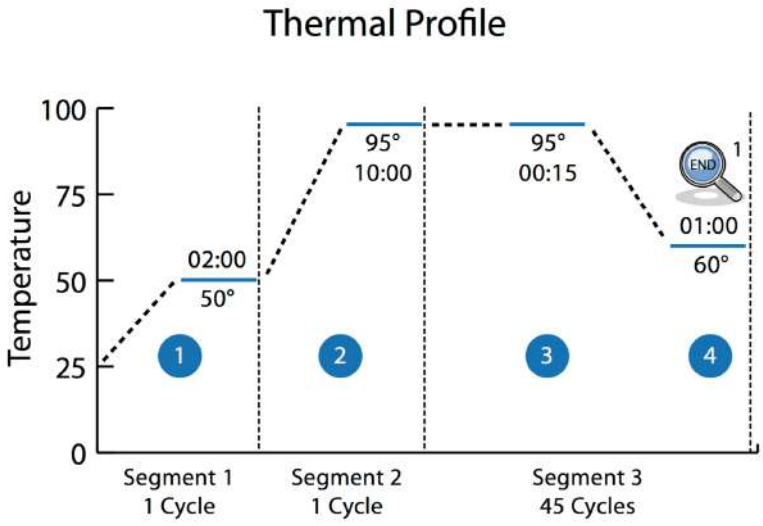

Figure A.2: *Example of a thermal profile. The amplification curve will be performe on the segment 3. Reproduced from [63]*

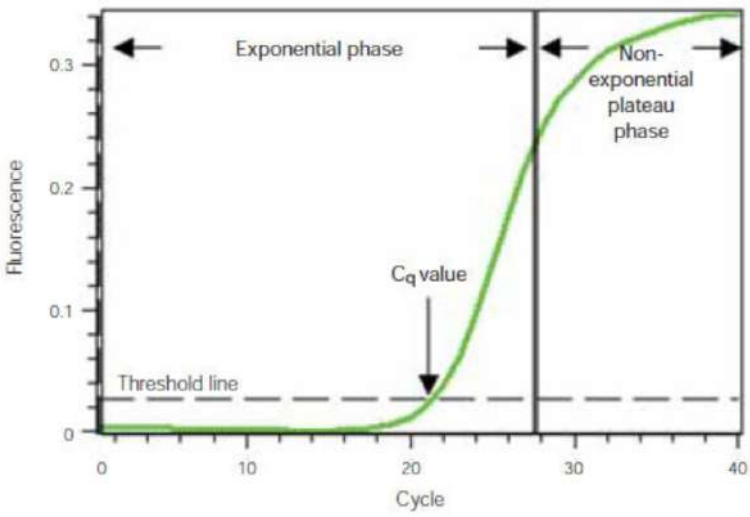

Figure A.3: *Example of amplification curve.*

level in the early cycles, when there is no detectable increase in fluorescence, due to PCR products.

- The threshold is the level of fluorescence above the baseline, at which the signal can be considered not to be background.
- The Ct value is defined as the cycle in which there is a significant increase in reporter signal, above the threshold. It is consequently related to the initial amount of DNA and shows also the sensitivity of the assay. The Ct value is

consequently in inverse proportion to the expression level of the gene. The Ct is therefore dependent on the threshold level, and it is then important to compare the threshold value from one run to another, if no normalization method is used.

The normalization and quantification will be present in the results of this report.

Western Blot

The term blotting refers to the transfer of biological samples from a gel to a membrane and their subsequent detection on the surface of the membrane. Western blotting - WB (also called immunoblotting because an antibody is used to specifically detect its antigen) was introduced by Towbin, in 1979 and is now a routine technique for protein analysis. The specificity of the antibody-antigen interaction enables a target protein to be identified in the midst of a complex protein mixture. Western blotting can produce qualitative and semiquantitative data about that protein [64].

WB is often used in research to separate and identify proteins. In this technique a mixture of proteins is separated based on molecular weight, and thus by type, through gel electrophoresis. These results are then transferred to a membrane producing a band for each protein. The membrane is then incubated with labels antibodies specific to the protein of interest.

The bound antibodies are then detected by developing the film. As the antibodies only bind to the protein of interest, only one band should be visible. The thickness of the band corresponds to the amount of protein present [65].

The first step in a WB procedure is to separate the macromolecules using gel electrophoresis. After electrophoresis, the separated molecules blotted onto a second matrix, generally a nitrocellulose membrane. The membrane is blocked to prevent any nonspecic binding of antibodies to the surface of the membrane. The transferred protein is complexed with an enzyme labeled antibody as a probe. An appropriate substrate is then added to the enzyme and together they produce a detectable product such as a chromogenic precipitate on the membrane for colorimetric detection. The most sensitive detection methods use a chemiluminescent substrate that, when combined with the enzyme, produces light. The intensity of the signal should correlate with the abundance of the antigen on the blotting membrane.

- Electrophoresis Gel: The gel is typically cast in buffer containing sodium dodecyl sulfate (SDS) and protein samples are heated with SDS before electrophoresis so that the charge-density of all proteins is made roughly equal. Heating in SDS denatures proteins in the sample and SDS binds tightly to the uncoiled protein molecule. So, when samples are electrophoresed, proteins separate according to the mass.

- Electro-Transfer: After electrophoresis, the protein must be transferred from the gel to a membrane. The transfer method that is used most commonly for proteins is electrophoretic transfer because of its speed and transfer ef ciency.

- Blocking: To block the unreacted sites on the membrane and reduce the nonspecic binding of proteins during subsequent steps. The blocking buffer should improve the sensitivity of the assay by reducing background interference. The proper choice of blocker for a given blot depends on the antigen and on the type of enzyme conjugate to be used. The ideal blocking buffer will bind to all potential sites of nonspecic interaction, eliminating background.

- Primary Incubation: The choice of a primary antibody for a Western blot will depend on the antigen to be detected and what antibodies are available to that antigen.

- Wash: WB consists of a series of incubations with different immunochemical reagents separated by wash steps. Washing steps are necessary to remove unbound reagents and reduce background. It can be performed in a physiological buffer such as Tris-buffered saline (TBS) or phosphate-buffered saline (PBS) without any additives.

- Secondary Incubation: A secondary antibody aids in the detection, sorting or purification of target antigens by binding to a primary antibody, which directly binds to the target antigen. Secondary antibodies offer increased sensitivity through the signal amplication. After the second antibody the membrane need to be wash again.

- Incubation with Substrate: The appropriate substrate choice depends on the enzyme label, desired sensitivity, and desired form of signal or method of detection. Chromogenic substrates or chemiluminescent substrates are widely used and offer perhaps the simplest and most cost-effective method of detection.

- Target Detection: There are several methods for capturing data generated from WB, including X-ray, cooled CCD cameras and phosphorimagers. Cooled CCD cameras, which offer the advantages of instant image manipulation, greater resolution and a larger dynamic range, also eliminate the need for a darkroom and processing equipment.

After the image acquisition it can be treat using a software that correlate the intensity of the signal with the abundance of the antigen on the blotting membrane.

Methodology

The methodology present in this chapter include the cell culture, hypoxia, microRNA extraction, electrophoresis gel, qPCR and Western blot experiments.

Cell line and culture

The experiments were performed with MCF-7 cells from American Type Culture Collections (ATCC; Middlesex, UK). The cell lines were cultured in their respective growth media in cell culture flasks according to their manufacturers recommendations.

Before start the experiments all solutions and equipment were sterile and all the solutions were pre-warmed.

The cell grown in a culture vessel (T25) with cell culture media supplemented with 10% Fetal Bovine Serum, 1% L-Glutamine and 1% penicillin-streptomycin solution, incubated at 37°C, 5% CO_2.

When the cells become confluence, the culture media was removed and the flasks were wash with Phosphate Buffered Saline (PBS). MCF7 are adhering cells and in order to remove them from the bottom of the flasks a small amount of trypsin was add and the flask was incubated at 37°C for approximately 5 minutes.

The cells were observed under the microscope for detachment. If around 90% of the cells were detached, add 4mL growth medium. The medium was pipetted over

the cell layer surface several times. The grownth medium with cells was transfered to a 15mL conical tube and centrifuged at 1300 rpm for 5 minutes.

The cell pellet was resuspend in a volume of pre-warmed growth medium and pipetted the appropriate volume into new cell culture vessels, and returned the cells to the incubator. This steps are call passage.

Hypoxia Experiment

In order to evaluate the hypoxia, at least two identical twin cell cultures were prepare the day before as described above.

The tubes used for the injection/purging the hypoxic gas were attach to the chamber and gently opened the steel ring clamp. The cell culture were placed in the hypoxic chamber. Also place a Petri dish containing sterile water was add the chamber to provide adequate humidification. A twin cell culture was placed in normoxia as control in the same incubation.

The steel ring clamp was position to ensure the hermetical closure of the chamber and closed it. To create hypoxia, attach the tubing to a "hypoxia tank" containing a 1% O_2 5%CO_2 rest nitrogen gas mixture. The gas was opened tank at a flow rate of 20 liters per minutes for 4 minutes. Then quickly turned off the gas flow and completely close the chamber by closing both white clamps. The chamber was placed in the incubator for 48h.

microRNA extraction

The microRNA were extract from normoxia and hypoxia cells using the miRCURY RNA Isolation Kit - Cell & Plant from Exiqon.

The cells grew in monolayer and to detach them from the flasks was added trypsin, incubated and removed as described above. After centrifuge they were washed with PBS and centrifuge again. The PBS was removed, added 350μL of lysis solution and gently pipetted to mix and transfer the lysate to a microcentrifuge tube. Added 200 μL of 96 % ethanol to the lysate. Evething was mix by vortexing for 10 seconds.

A column with one of collection tubes was assembled and added 600 μL of the lysate with the ethanol onto the column and centrifuged for 1 minute at 3 500 x g. The flowthrough was discated and reassembled the spin column with its collection tube.

400 μL of wash solution was added to the column and centrifuged for 1 minute at 14 000 x g. This step was repeated 2 more times by adding another 400 μL of wash solution and centrifuging for 1 minute at 14 000 x g. By the end, the column was spun for 2 minutes at 14 000 x g in order to thoroughly dry the resin.

The column was placed into a fresh 1,7 mL elution tube provided with the kit. Added 50 μL of elution buffer to the column and centrifuged for 2 minutes at 200 x g, followed by 1 minute at 14 000 x g. The purified RNA sample was stored at - 20°C for a few days when necessary.

qPCR

To perform the qPCR the miRCURY LNA Universal RT microRNA PCR kit was used. It is based in two steps:

1. One first-strand cDNA synthesis reaction provides template for all microRNA real-time PCR assays.

2. Real - time PCR amplification with the specific primer to microRNA expression profiling and for quantification of individual microRNAs.

This procedure can be ilustrate in Figure 4.1 and will be describe with more details in sequence.

Concentration

The concentration of microRNA extracted previously was adjusted to a concentration of 5 ng/μL using nuclease free water. The value was checked using a NanoDrop Spectrophotometer with absorbance spectra at 260nm.

First is necessary to calculate de number of samples or wells that will be used. Each plate well will be full with 10μL of reverse transcription (RT) working solution. The RT solution was prepared according Table 4.1.

After prepare the required amount of RT solution it was placed on ice. The RT solution was dispensed into nuclease free tubes, mixed very gentle vortexing and spun down.

The tubes were incubated for 60 min at 42°C. Heat-inactivated the reverse transcriptase for 5 min at 95°C and immediately cooled to 4°C. Stored at 4°C or freeze if it is necessary.

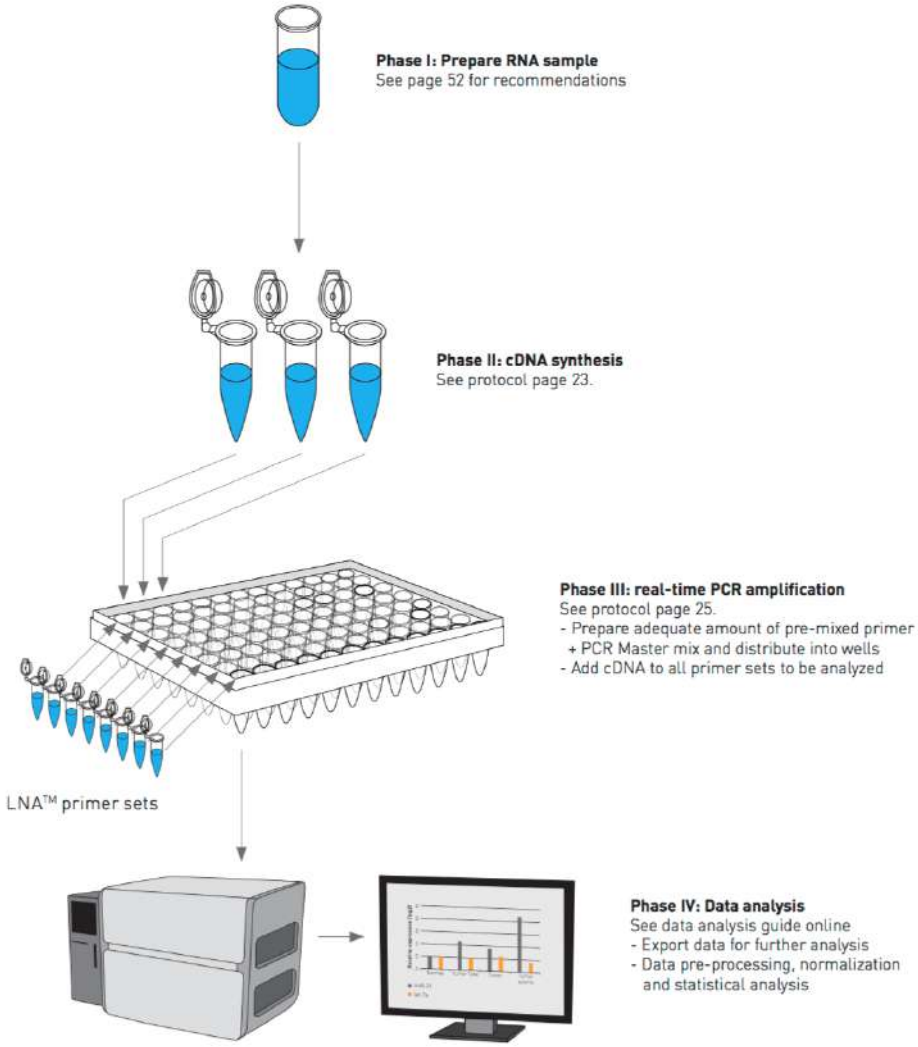

Figure A.4: *Workflow for qPCR*

The amount of cDNA template needed for the planned real-time PCR reactions was diluted 80x in nuclease free water.

To prepare multiple real-time PCR reactions with the same microRNA primer set, the master mix working-solution of the PCR primers and the PCR Master mix were prepared according to Table 4.2:

The required amount of primer was prepared and placed it on ice. The relevant volume of primer was placed in PCR wells and spun plate briefly in a centrifuge (1500g for 1 minute), to remove air bubbles. The cDNA template was

Reagent	Volume (μL) RT reaction
5x Reaction buffer	2
Nuclease-free water	4.5
Enzyme mix	1
Synthetic RNA spike	0.5
Template total RNA	2
total volume	10

Table A.1: *Reverse transcription reaction setup.*

Reagent	Volume (μL)
PCR Master mix	5
PCR primer mix	1
Diluted cDNA template	4
total volume	10

Table A.2: *Real - time PCR reaction, pr. 10μL reaction.*

added to each well.

The plate was sealed with optical sealing and centrifuged. The qPCR amplification was performed followed by melting curve analysis according to Table 4.3.

Process step	Settings
Polimerase activation	95°C, 10min
Amplification	45 amplifications cycles 95°C 10s, 60°C 1min

Table A.3: *Real-time PCR cycle conditions*

CT values were automatically determined by the Step One Plus^{TM} Real-Time PCR system (Life Technologies, UK). Relative expression of target mRNA in different samples were normalised to a set of reference genes.

The use of reference genes as endogenous controls in qRT-PCR is one of

the most common methods used in the normalization of qRT-PCR data. However, the expression of reference genes may vary considerably between experiments as no single gene is stably expressed from sample to sample or under all experimental conditions.

Agarose gel electrophoresis

MicroRNA can be separate using molecular grade agarose. A 2% agarose gel was prepared by dissolving agarose powder in 1x TAE buffer and heating in a microwave until the agarose powder was dissolved in the buffer. Ethidium bromide (10mg/ml) was added to a final concentration of 0.5μg/mL and the solution was poured into a gel tray and left to set at room temperature for 15 minutes. DNA samples were loaded onto the gel and subjected to electrophoresis at 120V for 1 hour. DNA hyperladder run simultaneously to allow estimation of DNA fragment sizes. DNA was visualised under UV light on a MiniBis gel documentation system.

Western blot

The cells in normoxia and hypoxia were analysed by Western blot technique.

Before star the experiment it is necessary to prepare all the buffers as described:

1. RIPA + PI
   One tablet protease inhibitor (PI) to 10mL of RIPA buffer.

2. 10x running buffer (1L)
   30g Tris (250mM) +140g glycine (1.9M) + 10g SDS made up to 1L with D.I. water. pH 8.3

3. 1x running buffer (700ml)
   70mL 10x running buffer + 630mL D.I. water

4. 10x transfer buffer (1L)
   30.29g Tris (250mM) + 142.63g glycine (1.9M) made up to 1L with D.I. water

5. 1x transfer buffer (1L)
   100mL 10x transfer buffer + 200mL methanol + 700mL H2O

6. 10x TBS (1L)
   Dissolve 60.6g Tris + 87,6g NaCl in 600mL D.I. water. Add 100mL of dilute HCl (1N). pH to 7.6 with HCl. Make up to 1L with D.I. water.

7. Buffer A (200mL)
   36.34g Tris (1.5M) in 150mL dH2O, pH to 8.8 and make up to 200mL

8. Buffer B (200mL)
   24.23g Tris (1M) in 150mL dH2O pH to 6.8 and make up to 200mL

The cells were removed from the flasks and washed with phosphate buffered saline (PBS) as already described. After centrifuge 500-1000μL RIPA + PI buffer were added to the cells and put in Eppendorf tube on ice for 30 mins. Frozen-thaw 3 times. Spun down for 15 mins at 12,000 RPM at 4°C. The cells was apellet and the supernatant was protein. The supernatant was tranfered to fresh 1.5mL tubes and the pellet was discarded.

To prepare BSA (bovine serum albumin) was added 2mg in a 1.5mL. Added 1mL of nuclease-free water. And prepared four 1.5mL tubes diluting it into 1mg, 0.5mg, 0.25mg and 0.125mg. 30μL of stock protein was diluted with 30μL water.

To determine the total volume of working reagent (WR) required the equation was used: (# standards + # unknowns) x (# replicates) x (volume of WR per sample, 0.2mL) = total volume WR required.

WR was prepared by mixing 50 parts of BCA reagent A with 1 part of BCA Reagent B (50:1, Reagent A: B). In a 96 well culture plate 25μL of standard/sample/blank was added in each well in triplicate.

200 μL of the WR was added to each well and placed on a shaker for 30 seconds to mix. The plate was covered with foil and placed at 37°C in the incubator for 30 minutes. After cooled the plate to room temperature, the absorbance at or near 562nm was verified on a plate reader generating a standard curve to read off proteins concentration (from 2mg to 0.125mg).

The gel for electrophoresis is compouse by two parts: stack gel on the top and separating gel. They were prepared according to the Table 4.4

The running buffer was prepared with 900mL Milli DI water and 100mL 10X running buffer stock. And for 1-3 gels 800mL of running buffer was used. Overlaid

	Stack Gel	Separating Gel
30% Acrylamide mix	0.67mL	3.3mL
Buffer A		2.5mL
Buffer B	0.5mL	
Water	2.4mL	4.1mL
10% ammonium persulfate (APS)	100μL	100μL
TEMED	40μL	40μL

Table A.4: *Acrylamine gel preparation.*

with stack gel and placed a 10 or 15 well comb.

The protein was prepared in 1:1 ratio of lamelli buffer. Loaded 20μg per well. Boiled at 100°C on heat block for 5 mins then hold on ice for at least 3 minutes. The samples were loaded to wells, along with protein marker and controls.

The tank was filled up until the middle with 1x running buffer and 100V was applied for 1 hour.

To do the wet transfer 1L transfer buffer is necessary (100mL 10x transfer buffer + 200mL methanol + 700mL Milli DI water).

6x blotting paper and 1x PVDF membrane to size (7 x 8.5 x 6 cm) were cut. It is necessary to remember scribe what the membrane is for identification in pencil and cut the top left hand corner off to know which way round it goes and which side has the proteins.

The membrane was actived in methanol for 5 mins and washed for 3 mins. The blotting paper and cassette sponges were left on ice cold transfer buffer. Carefully the stacking gel was removed from the acrylamide gel. To assemble the cassette in a dish with transfer buffer (from bottom up) in the follow sequence was used: black side down, sponge, 3 sheets of blotting paper, gel, membrane, 3 sheets of blotting paper (roll with a roller to get rid of air bubbles), sponge and the red side, as you can see in Figure 4.2.

A freezer pack was placed into the transfer tank and 100V potencial was applied for 1 hour.

First, the following solutions were made:

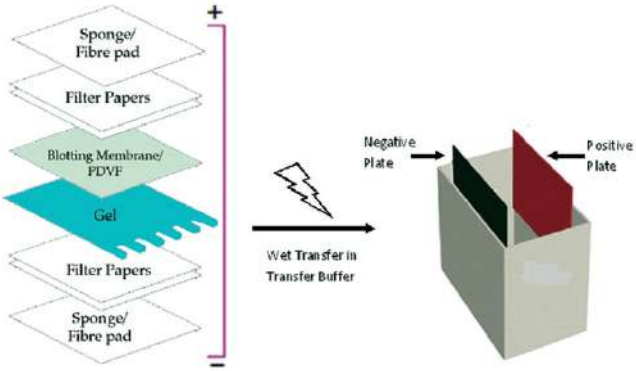

Figure A.5: *Assembly of a sandwich in Western Blot. Reproduced from [65].*

1. TBS-T: 100ml 10xTBS, 900ml Milli DI water and 500μl Tween-20.

2. 5% Blocking Solution: 2.5g milk powder and 50ml TBS-T.

The membrane was block in 5% blocking solution for 1 hour at R and incubated overnight at 4°C in primary antibody solution on a roller or shaker.

In the next day, the membrane was washed 3 times in 1xTBST for 10 mins. The secondary antibody (1:5000) was added (1μl antibody in 5mL blocking solution). The membrane was incubated in secondary antibody for 1 hour at room temperature on shaking machine. Washed 3 times in 1xTBST for 5 mins.

The final procedure need to be done on the dark room. The membrane was incubated in 1000μL of substrate for 1 minutes, cleaned and placed on the cassette. A plastic acetate sheet was used to cover the membrane.

The lights need to be turned off at this point. The film box has to be open in the dark to remove one sheet. This film was placed over the membrane and marked the top and side on the plastic acetate to help to draw your ladder later.

The film was exposed for 30s initially. After the exposure period, the film has to be develop in the developer solution checking it every 5 seconds until the bands appear. After that, the film was washed quickly in the water before placing it in the fixer for 15 seconds. Placed again in water. Washed under the sink and air dried.

Results

This section will present the main results divided according to the technique.

Cell Culture

The cell cultures started with one flask of MCF-7 cells. The cells grown and were replicated after get confluent. Normally, once a week until they were enought to start the experiments in T25 flaks, as Figure 5.1:

Figure A.6: *Cell culture flasks before incubation.*

The cells are adherent, which means that they grown as monolayers on an artificial substrate will not be free-floating in the culture medium. In Figure 5.2 show the confluent MCF-7 cells 6 days after the passage.

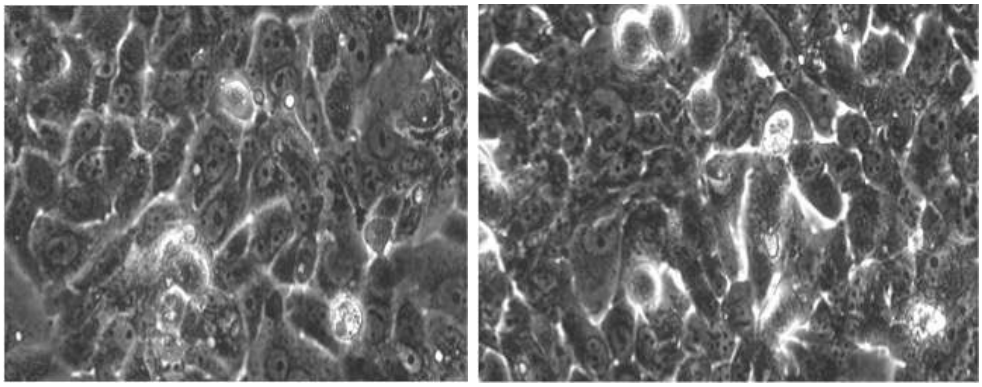

Figure A.7: *MCF-7 cells confluent. Passage number 28.*

By the middle of April after one of the passages where the cells where diluted in a lower concentration they started to grown really slow. Not all cell lines grown

fine in low concentration. The distance between them can favor the comunication. After 2 or 3 weeks the cells went back to the normal grown.

During all cell culture no contamination was notice.

Hypoxia

As hypoxia affects a variety of tumor-associated events including in breast cancer. The number of miRNAs are differentially expressed in response to hypoxia. The same happens with proteins. To evaluate different miRNA and protein expression with MCF 7 cells in normoxia and hypoxia conditions using different techniques.

A simples picture of cell culture after 48h in hypoxia is present in Figure 5.3. No significant changes can be observed.

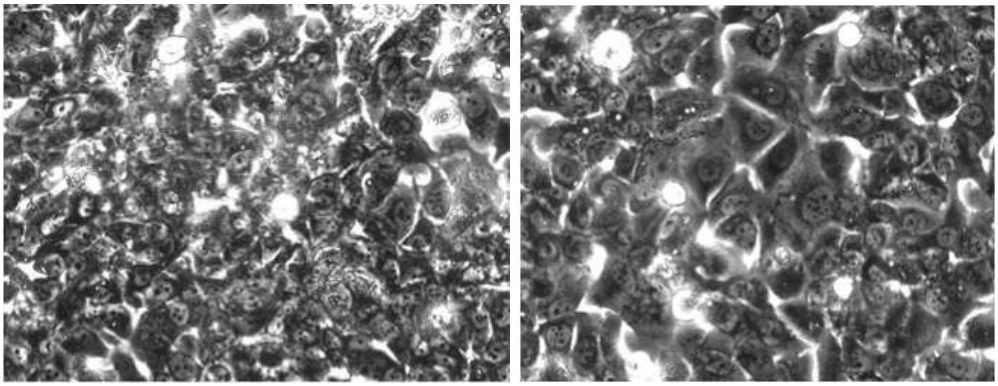

Figure A.8: *MCF-7 cells confluent and after 48h in hypoxia. Passage number 28.*

The miRNA from normoxia and hypoxia cell culture were extract and evaluated using electrophoresis and qPCR.

Electrophoresis Gel

Electrophoresis is a technique used in order to separate macromolecules based on size. Figure 5.4 presents the ladder on the left and the samples on the right. In this case ,two different passages of MCF-7 cells in normoxia, P22 and P23. The size of the miRNA fragments can be compared with the ladder. The same ladder were used in all electrophoresis experiments.

In this case, two different size of fragments can be observed. The different in intensity between the samples are related with the amount of miRNA extract from each one.

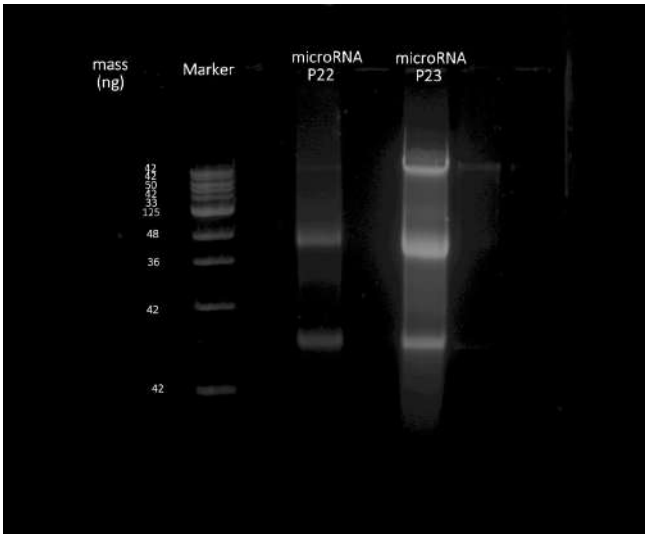

Figure A.9: *Electrophoresis gel tested with microRNA extracted from MCF7 cells in different passages.*

Throughout the months, three groups of MCF-7 cells were analyzed. All them come from the same cell line, but are in different passage to check if this parameter can affect the miRNA expression.

Figure 5.4 synthesizes the results. In the left there is the ladder. The samples can be divided in couples. P refers to the cell passage, and there is three different passages (8, 31 and 33). H refers to hypoxia and C to control. The experiment was repeates twice. In this case, the miRNA extract present the same fragments. The electrophoresis gel has not only the miR-200a, but all the miRNA extract from the cell culture.

Numerous studies show miRNAs with oncogenic and tumor suppressive signatures correlated with various types of cancer and, in particular, the miRNAs interact with conditions in the tumor microenvironment, such as hypoxia. Recently, a few reports revealed that miRNAs were associated with several key signaling pathways that respond to hypoxia and played important roles in hypoxic adaptation including miR-200a. This specific miRNA was found to be down-regulated, in response to hypoxia [66].

However, the miR-200a can not be analyzed just looking to the band in Figure 5.5. To verify the expression and quantify, qPCR was employed.

qPCR

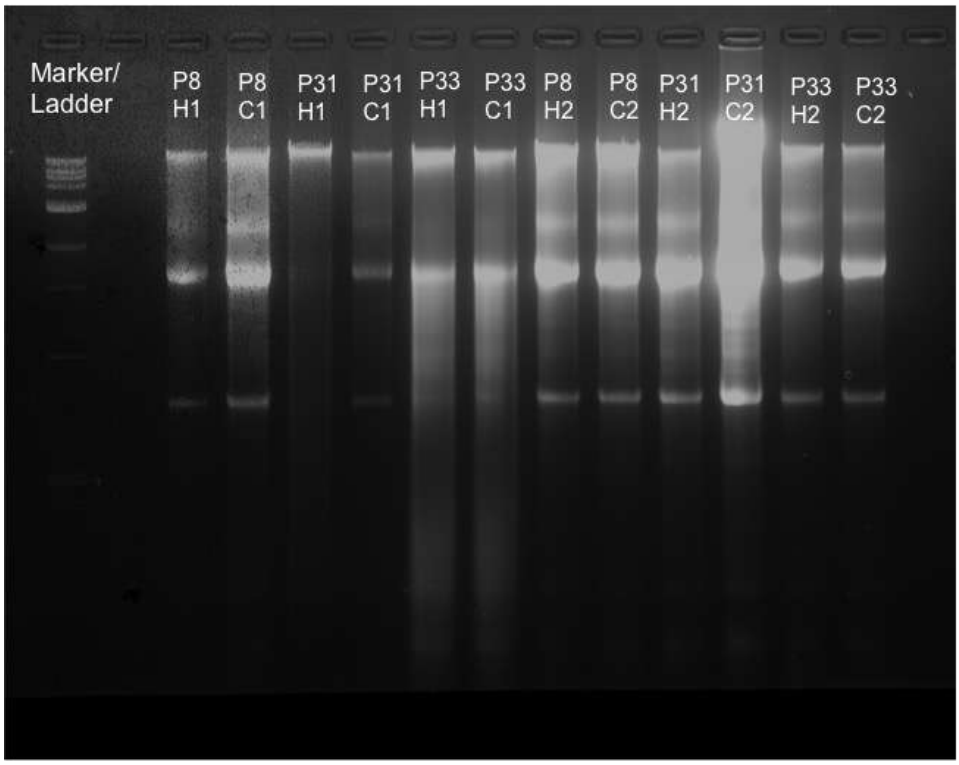

Figure A.10: *Electrophoresis gel tested with microRNA extracted from MCF7 cells in different passages. The P represents the passage, H hypoxia and C control or normoxia. The experiment was repeated twice.*

The Real-Time experiments has to deal with several uncontrolled variables, as the amount of starting material, enzymatic eficiencies, and differences between tissues, individuals or experimental conditions. In order to make a good comparison, normalization can be used as a correction method, for these variables. The most commonly known and used ways of normalization are housekeeping genes and using internal or external calibrator.

Normalization using housekeeping gene excludes some of the above-mentioned drawbacks, but is also not the perfect method. The advantage is that the variation due to different amounts of RNA can be excluded. However, one must assure oneself, that the housekeeping gene is expressed constantly at the same level throughout the experiment and between samples. In relative quantification, the expression of the gene of interest in a sample is expressed relatively to another gene, another sample, used as a reference [63].

In Figure 5.6 the amplification curve is present to compare the miR-200a

(red) to the housekeeping gene curve (blue).

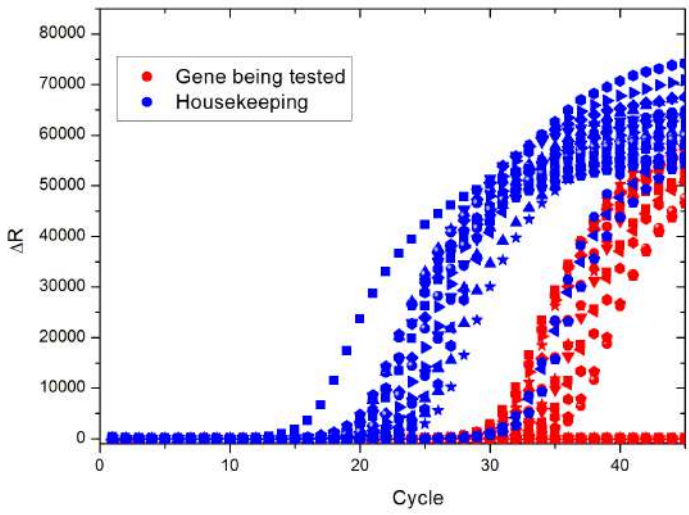

Figure A.11: *Amplicification curve for 45 cycles. In blue are the curves from microRNA 200a being tested and in red the housekeeping gene for normalization.*

To analyze the data, one of the most comum methods "delta delta Ct" (ΔΔCt) method will be explain here. This method is the simplest one, as it is a direct comparison of Ct values between the target gene and the reference gene. However, PCR efficiencies of both gene should be close to 100 % and not differ by more than 10 %.

Firstly, the ΔCt between the target gene and the reference gene is calculated for each sample:

$$\Delta Ct = Ct_{target} - Ct_{reference} \tag{A.1}$$

Then the difference between the ΔCt of the unknown and the ΔCt of the calibrator is calculated, giving the ΔΔCt value:

$$\Delta\Delta Ct = (Ct_{target} - Ct_{reference})_{calibrator} - (Ct_{target} - Ct_{reference})_{sample} \tag{A.2}$$

The normalized target amount in the sample is then equal to $2^{-\Delta\Delta Ct}$ and this value can be used to compare expression levels in samples.

The Tables 5.1 present jst one of the data obtain from qPCR and the ΔΔCt method applied to them as an example to the cells in passage 5:

	Exp. Ct	Con. C.	Exp. ΔCt	Cont. ΔCt	ΔΔCt	$2^{-\Delta\Delta Ct}$
Housekeeping Gene	21.43	20.66	1.88	4.0	-2.12	4.35
Gene being Tested	23.31	24.67				

Table A.5: *Example of data analize from P5 cells. The Exp. Ct and Con. Ct values are the average of three results.*

In the Table 5.1, the Exp. Ct and Con. Ct values are the average of three experiments. Ct values less than 29 are strong positive reactions indicative of abundant target nucleic acid in the sample.

Table 5.2 show the ΔΔCt and $2^{-\Delta\Delta Ct}$ values to different cell passage.

Passage	ΔΔCt	$2^{-\Delta\Delta Ct}$
P5	-2.12	4.35
P28	- 2.16	4.45
P30	-2.12	4.35

Table A.6: *ΔΔCt and $2^{-\Delta\Delta Ct}$ values to different cell passage without use any passive reference dye.*

The Exiqon kit used to qPCR analysis do not come with a component to normalize the fluorescence. One other experiment was repeated adding ROX passive reference dye to the wells.

Passage	ΔΔCt	$2^{-\Delta\Delta Ct}$
P8	1.10	0.46
P30	- 2.09	4.26
P32	-2.12	4.35

Table A.7: *ΔΔCt and $2^{-\Delta\Delta Ct}$ values to different cell passage using ROX as passive reference dye.*

Western Blot

One other techniques helpful to evaluate changes in protein expression is Western Blot [65]. For example, HER2 proteins are receptors on breast cells that

control how a healthy breast cell grows, divides, and repairs itself. But in 25% of breast cancers, the HER2 gene doesn't work correctly and breast cells grow and divide in an uncontrolled way. Breast cancers with HER2 gene amplification or HER2 protein overexpression are called HER2-positive.

HER2 was tested in the first part of this project at University of Bath to develop a biosensor. However, MCF7 are HER2 negative, what means that this cell line does not have a overexpression of this protein. In this case, we could evaluate CA protein in normoxia and hypoxia conditions, using the M75 as antibody.

The principal aim of this experiments is learn one other technique that could be used to compare the values with a future biosensor.

After the procedure described in the Methodology, the Figure 5.7 representes the result. The experiment was repeted twice. In both of them the sequence of the columns are the same. P means the passage, H hypoxia and C control or normoxia.

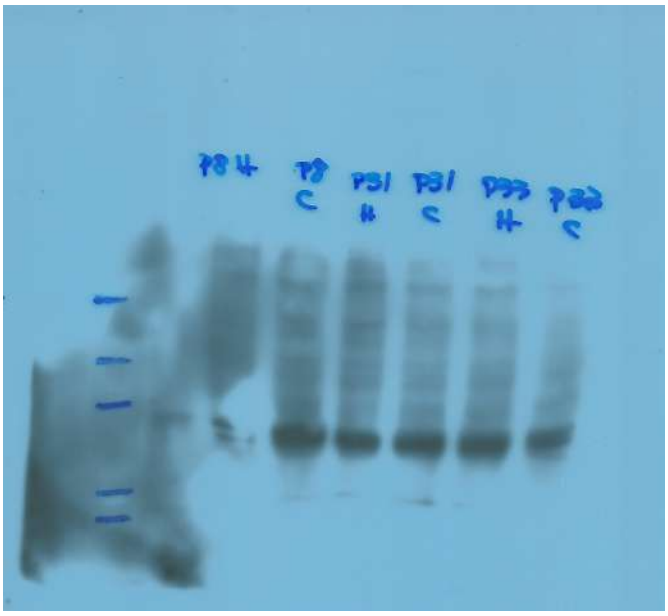

Figure A.12: *Western Blot result for MCF7 cells exposed to hypoxic conditions.*

According to the literature, MCF7 cells exposed to hypoxic conditions has a increase of protein expression. If we have this increase, the band in WB should be thicker in hypoxic conditions when compare to normoxic. Actually, no difference could be observed. One of the reasons can be the difficult do perform the Western Blot, since it is a quiet complicated technique.

Conclusions

In this collaborative part of the project focus on biological analize and quantification of microRNA and proteins.

In biological research the common techniques to analize DNA, RNA and protein were explored in this collaboration. Since the basic things as cell culture, passages and extraction from flasks follow by miRNA extraction were develop.

Electrophoresis gel was employed to check the fragments after miRNA extraction in normoxia and hypoxia. The specific miRNA used as probe in this owrk, miR-200a, was analized using qPCR. The results give the idea about how to compare the biosensor detection to standard techniques. To improve the aptsensor ideia the Western Blot technique was tested with different conditions.

Finally, all biological standard techniques were employed to understand how the biosensor can be compare with them. Also, different cell condicions, as hypoxia, was tested to undersatand one of the factors that can affect miRNA and protein expression.